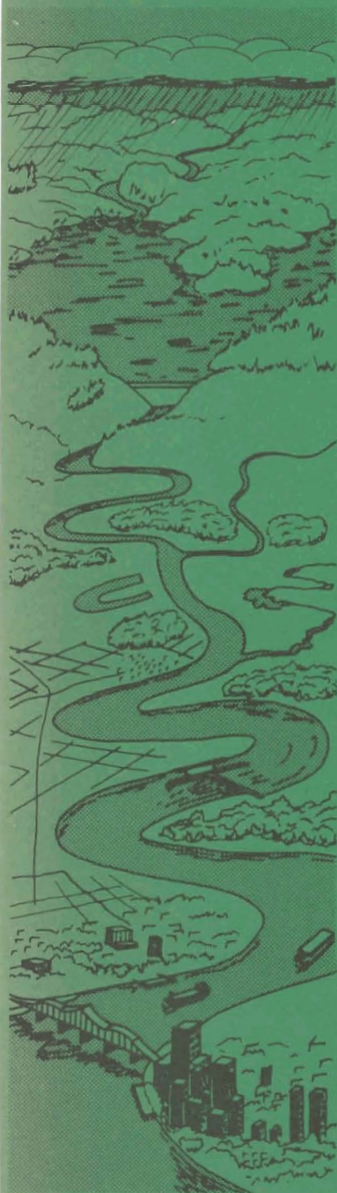




US Army Corps
of Engineers



GRACE

ENVIRONMENTAL & WATER QUALITY
OPERATIONAL STUDIES

TECHNICAL REPORT E-83-7

AN ASSESSMENT OF
RESERVOIR DENSITY CURRENTS
AND INFLOW PROCESSES

by

Dennis E. Ford

Ford, Thornton, Norton, and Associates, Ltd.
P. O. Box 927
Vicksburg, Miss. 39180

and

Marc C. Johnson

Environmental Laboratory
U. S. Army Engineer Waterways Experiment Station
P. O. Box 631, Vicksburg, Miss. 39180



July 1983

Final Report

Approved For Public Release; Distribution Unlimited

Prepared for Office, Chief of Engineers, U. S. Army
Washington, D. C. 20314

Under Purchase Order No. DACW39-82-M-2042
(EWQOS Task IA)

Monitored by Environmental Laboratory
U. S. Army Engineer Waterways Experiment Station
P. O. Box 631, Vicksburg, Miss. 39180

Unclassified

SECURITY CLASSIFICATION OF THIS PAGE (When Data Entered)

REPORT DOCUMENTATION PAGE		READ INSTRUCTIONS BEFORE COMPLETING FORM
1. REPORT NUMBER Technical Report E-83-7	2. GOVT ACCESSION NO.	3. RECIPIENT'S CATALOG NUMBER
4. TITLE (and Subtitle) AN ASSESSMENT OF RESERVOIR DENSITY CURRENTS AND INFLOW PROCESSES		5. TYPE OF REPORT & PERIOD COVERED Final report
		6. PERFORMING ORG. REPORT NUMBER
7. AUTHOR(s) Dennis E. Ford and Marc C. Johnson		8. CONTRACT OR GRANT NUMBER(s) Purchase Order No. DACW39-82-M-2042
9. PERFORMING ORGANIZATION NAME AND ADDRESS Ford, Thornton, Norton, and Associates, Ltd. P. O. Box 927, Vicksburg, Miss. 39180 U. S. Army Engineer Waterways Experiment Station Environmental Laboratory P. O. Box 631, Vicksburg, Miss. 39180		10. PROGRAM ELEMENT, PROJECT, TASK AREA & WORK UNIT NUMBERS EWQOS Task IA
11. CONTROLLING OFFICE NAME AND ADDRESS Office, Chief of Engineers, U. S. Army Washington, D. C. 20314		12. REPORT DATE July 1983
14. MONITORING AGENCY NAME & ADDRESS (if different from Controlling Office) U. S. Army Engineer Waterways Experiment Station Environmental Laboratory P. O. Box 631, Vicksburg, Miss. 39180		13. NUMBER OF PAGES 110
		15. SECURITY CLASS. (of this report) Unclassified
		15a. DECLASSIFICATION/DOWNGRADING SCHEDULE
16. DISTRIBUTION STATEMENT (of this Report) Approved for public release; distribution unlimited.		
17. DISTRIBUTION STATEMENT (of the abstract entered in Block 20, if different from Report)		
18. SUPPLEMENTARY NOTES Available from National Technical Information Service, 5285 Port Royal Road, Springfield, Va. 22161.		
19. KEY WORDS (Continue on reverse side if necessary and identify by block number) Density currents Mathematical models Reservoirs Water quality		
20. ABSTRACT (Continue on reverse side if necessary and identify by block number) Since tributary inflows are usually the major sources of nutrients and other materials affecting reservoir water quality, techniques for predicting the characteristics of density currents can help the U. S. Army Corps of Engineers regulate the quality of reservoir and release waters. This report provides a literature review of density current predictive techniques, in which field observations, factors inhibiting prediction, (Continued)		

Unclassified

SECURITY CLASSIFICATION OF THIS PAGE(When Data Entered)

20. ABSTRACT (Concluded)

and water quality implications are discussed and predictive techniques are presented and analyzed. Specific equations for predicting plunge point location, initial mixing, interflow thickness, propagation speed, and underflow entrainment are developed and compared, and certain ones recommended for use.

A mathematical method for determining water density, example computations illustrating how to use the recommended predictive equations, and a relevant computer algorithm to be used in a one-dimensional water quality model (e.g., CE-QUAL-R1) are presented in appendices.

Unclassified

SECURITY CLASSIFICATION OF THIS PAGE(When Data Entered)

PREFACE

This report was prepared as part of the Environmental and Water Quality Operational Studies (EWQOS) Program, Work Unit IA, Develop and Verify Techniques for Describing Inflow Mixing Processes. The EWQOS program is sponsored by the Office, Chief of Engineers, and is assigned to the U. S. Army Engineer Waterways Experiment Station (WES), under the purview of the Environmental Laboratory (EL). Dr. J. L. Mahloch, EL, is the Program Manager of EWQOS.

The study was conducted during the period 1978 to 1982 by Dr. Dennis E. Ford and Mr. Marc C. Johnson of the Water Quality Modeling Group, Environmental Research and Simulation Division (ERSD), EL. The report was prepared for WES under Purchase Order No. DACW39-82-M-042 dated 3 March 1980 by Ford, Thornton, Norton, and Assoc., Ltd., Vicksburg, Mississippi. Mr. Johnson worked under the general supervision of Mr. D. L. Robey, Chief, ERSD, and Dr. John Harrison, Chief, EL.

The authors wish to acknowledge the valuable technical assistance provided by Mr. Mark S. Dortch of the Reservoir Water Quality Branch (Physical), Hydraulic Structures Division, Hydraulics Laboratory, during the course of this study.

The Commander and Director of WES during the preparation and publication of this report was COL Tilford C. Creel, CE. The Technical Director was Mr. F. R. Brown.

This report should be cited as follows:

Ford, D. E., and Johnson, M. C. 1983. "An Assessment of Reservoir Density Currents and Inflow Processes," Technical Report E-83-7, prepared by Ford, Thornton, Norton, and Associates, Ltd., and the Environmental Laboratory, Waterways Experiment Station, for the U. S. Army Engineer Waterways Experiment Station, Vicksburg, Miss.

CONTENTS

	<u>Page</u>
PREFACE	1
PART I: INTRODUCTION	3
PART II: BACKGROUND	4
Qualitative Description	4
Field Observations	8
Complicating Factors	12
Water Quality Implications	27
Discussion	30
PART III: PREDICTIVE TECHNIQUES	33
Overflows	33
Plunge Point Analysis	40
Initial Mixing and Entrainment	55
Underflows	60
Interflows and Intrusions	64
PART IV: SUMMARY AND RECOMMENDATIONS	71
Review Summary	71
Predictive Techniques	72
REFERENCES	75
APPENDIX A: DENSITY OF WATER	A1
APPENDIX B: EXAMPLE COMPUTATIONS	B1
APPENDIX C: COMPUTER ALGORITHM	C1
APPENDIX D: NOTATION	D1

AN ASSESSMENT OF
RESERVOIR DENSITY CURRENTS
AND INFLOW PROCESSES

PART I: INTRODUCTION

1. When a reservoir is formed by impounding a free-flowing river, both the flow regime and ecosystem characteristics change. The type of ecosystem that develops, the resultant water quality, and the ability to meet project purposes is dependent on understanding how inflows enter and pass through impoundments. Since tributary inflows are usually the major sources of materials such as nutrient and suspended and dissolved matter which impact reservoir water quality, techniques for predicting the characteristics of density currents are required to determine the ways in which management and operational alternatives can regulate reservoir and release water quality.

2. The objectives of this study were to:

- a. Review the literature and field studies on density currents in reservoirs.
- b. Develop techniques for predicting the placement, plunge point location, thickness, propagation speed, and mixing of density currents.

3. The predictive techniques include both simple computational equations (e.g., to calculate how fast a density current will move through a reservoir under the influence of a specific set of circumstances) and formalized algorithms for complex water quality models (e.g., CE-QUAL-R1 (Environmental Laboratory 1982)). The predictive techniques must, therefore, be sufficiently general to encompass the many different reservoir types operated by the U. S. Army Corps of Engineers (CE) and also be formulated on data and measurements routinely available for CE reservoirs.

PART II: BACKGROUND

4. Since the tributary inflow density usually differs from the density of the reservoir surface water, inflows enter and move through reservoirs as density currents. Bell (1942) defines a density current as "a gravity flow of a liquid or a gas through, under, or over a fluid of approximately equal density." Density flows differ from normal fluid flows because the buoyancy of the surrounding fluid reduces the gravity force by the normalized density difference, $\Delta\rho/\rho$ (i.e., reduced gravity force = $\frac{\Delta\rho}{\rho}g$). Vertical movements such as waves are therefore greater at the density interface than at the air-water interface. Katabatic winds, dust storms (e.g., Sudan haboob), sea breezes, and the advancement of a cold front are other examples of naturally occurring density currents.

5. In reservoirs, density currents are caused by density differences due to temperature, total dissolved solids (TDS), and suspended solids (SS). In most reservoirs, however, density differences are predominantly caused by temperature differences. For example, at 25°C it takes approximately 330 mg/l of dissolved solids or 420 mg/l of suspended solids (specific gravity = 2.65) to equal the density difference caused by a 1°C temperature change. Procedures to compute water densities based on temperature, TDS, and SS concentrations are presented in Appendix A.

Qualitative Description

6. When a tributary inflow enters a reservoir, it displaces the reservoir water ahead of it. Increases in water depth and cross-sectional area cause flow velocities to decrease. If there is no density difference between the tributary inflow and reservoir waters, the point of maximum velocity remains near the water surface as in open channel flow. The major forces acting on a parcel of water include the dynamic force exerted by the stream momentum and resisting force due to bed shear. Wind shear at the air-water interface can be either a

positive or negative force. As the inflowing parcel of water moves towards the dam, concentrations of inflowing constituents decrease due to diffusion and dispersion.

7. In most instances, the tributary inflows differ in density from the reservoir waters. Depending on the magnitude of this density difference, density currents can enter the epilimnion, metalimnion, or hypolimnion (Figure 1). When the inflow density is less than the surface water density, the inflow will float on the water surface (i.e., an overflow). In an overflow, the excess hydrostatic pressure in the density current causes the current to flow in all directions not obstructed by boundaries. Overflows are susceptible to mixing from wind-induced mechanisms and diurnal heating and cooling processes. Wind shear can direct the overflow into a cove or prevent it from moving downstream. Vertical mixing can also weaken the density difference by mixing the overflow throughout the water column, causing it to lose its integrity.

8. If the inflow density is greater than the water surface density, the inflow will push the reservoir water ahead until the buoyancy forces dominate and the inflow plunges beneath the water surface. The plunge point is sometimes made visible because of turbidity or the accumulation of floating debris, which may indicate a stagnation point. The location of the plunge point is determined by a balance between the stream momentum, the pressure gradient across the interface separating the river and reservoir waters, and the resisting shear forces. Some mixing (termed initial mixing) occurs at the plunge point because of the large eddies formed by flow reversals and pooling of the inflowing water (Akiyama and Stefan 1981). Knapp (1942) noticed that the flow in the vicinity of the plunge point occurred at the bottom of this pooled mixing zone (Figure 2). Ford et al. (1980) and Kennedy et al. (1983) substantiated this pooling phenomenon during dye studies on DeGray Lake, Arkansas, and West Point Reservoir, Georgia, when the dye clouds appeared to have stalled at the plunge point (Figure 3). The location of the plunge point can also be influenced by morphological factors. Changes in the

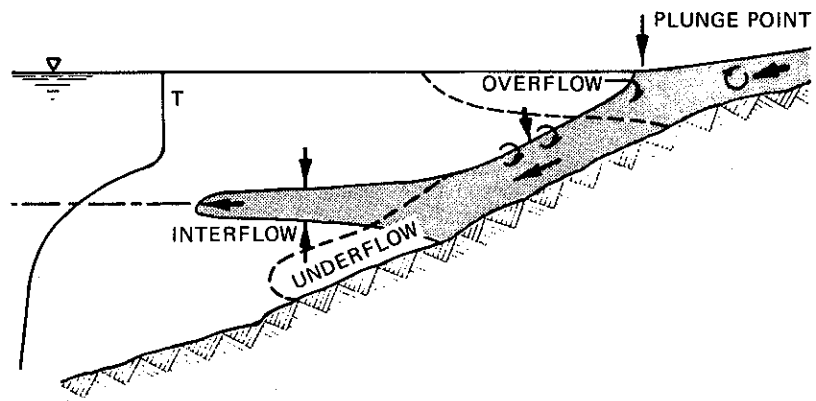


Figure 1. Density inflows to reservoirs.

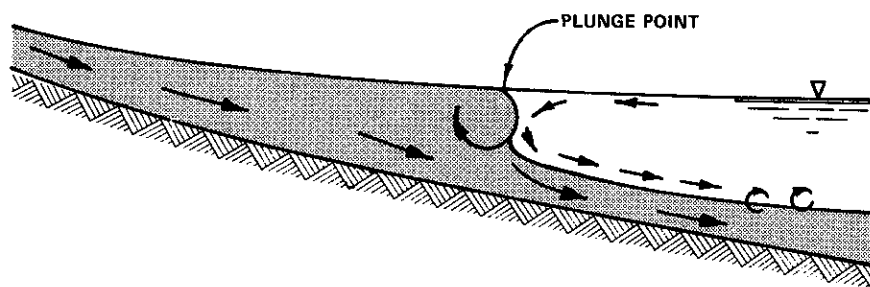


Figure 2. Pooling and mixing at plunge point.

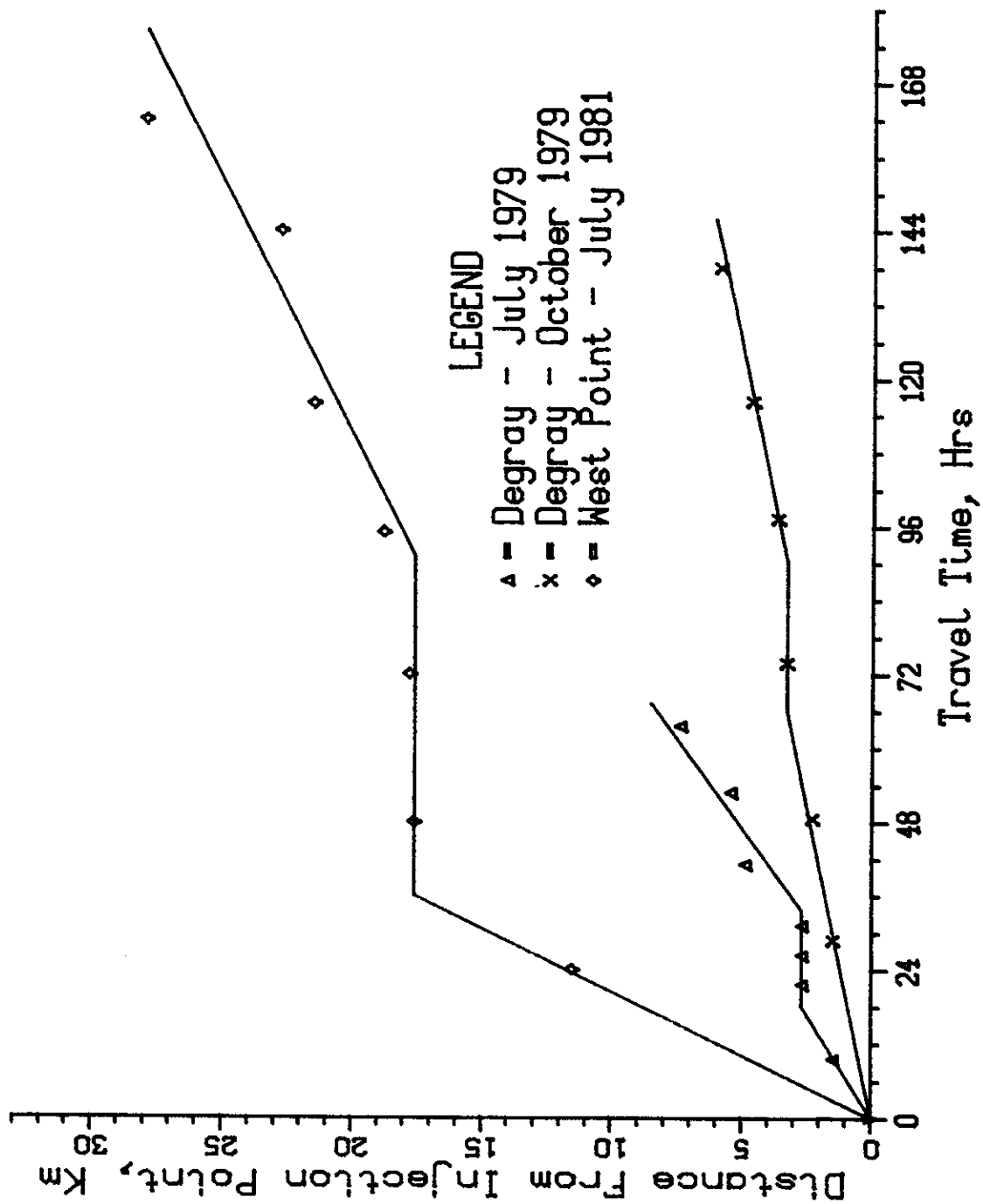


Figure 3. Movement of center of mass during three dye studies.

bed slope (e.g., due to sediment deposition), bed friction, and cross-sectional area may affect its location. For a river entering a wide lake, the plunge point may actually be a point rather than a line.

9. After the inflow plunges, it follows the old river channel (thalweg) as an underflow. The speed and thickness of the underflow is determined by a flow balance between the shear forces and the acceleration due to gravity (i.e., gradually varying flow theory). The momentum equation used in two-layered flow analysis is similar to the open-channel flow formulation except for the additional buoyancy force. An underflow will entrain overlying reservoir water due to turbulence generated by bottom roughness. Changes in the underflow density from entrainment must be quantified before a density interflow or intrusion can be analyzed, or the vertical placement of an interflow will be incorrect.

10. An interflow or intrusion occurs when a density current leaves the river bottom and propagates horizontally into a stratified body of water. Intrusions differ from overflows and underflows because an intrusion moves through a reservoir at a elevation where the intrusion and reservoir densities are similar. Intrusions require a continuous inflow and/or outflow for movement, or they stall and collapse (i.e., dissipate). Entrainment is usually neglected in the analysis of an intrusion since the density gradient in the metalimnion creates strong buoyancy forces which inhibit mixing.

Field Observations

11. The existence of density currents in reservoirs has been known for many years. Early studies consisted of watching turbid waters flow into a reservoir and disappear. Observations of turbid release water from Elephant Butte Dam, Rio Grande River, New Mexico, in the early 1900's indicated that turbid inflows could flow through a reservoir in a distinct layer (Grover and Howard 1938). Grover and Howard (1938) and accompanying discussions described the passage of silt-laden Colorado River water through Lake Mead, Nevada, based on chemical analysis of

inflow and outflow water. They suggested the possibility of increasing the life of a reservoir by promoting the passage of fine silt through reservoirs by bottom withdrawal. Wiebe (1939) suggested the existence of density currents in Norris Reservoir, Tennessee, based on routine limnological measurements including dissolved oxygen, alkalinity, pH, nitrite nitrogen, and turbidity.

12. Recent observations of density currents have been more quantitative using both naturally occurring substances and fluorescent dyes to trace density currents. Direct measurements of density currents have been limited since the velocities are below the detection limits of most current meters. The exception was the velocity measurements made by the Tennessee Valley Authority (TVA) using the DWICA isotopic current analyzer. These measurements were, however, time-consuming and therefore limited (Elder and Wunderlich 1972). Unsteady flow also made data analyses difficult.

Natural tracers

13. In many reservoirs, the properties of the inflowing streams are sufficiently different from the reservoir waters that the inflows can be tracked through the reservoir. Differences in turbidity, TDS, specific conductance, temperature, and other naturally occurring substances have all been used to trace inflows. Fry et al. (1953) documented density currents in 17 TVA reservoirs based on temperature, alkalinity, and chloride concentrations. The impact of these currents on industrial water use, stream pollution, recreation, municipal water supply, and steam plant condensing water was described in detail. In many cases, the density currents caused reverse currents which moved undesirable contaminants upstream into water intakes. Other studies of density currents in TVA reservoirs (e.g., Churchill 1958, Churchill 1965, Elder and Wunderlich 1972) described similar experiences. Other observations of density currents include Bighorn Lake, Montana (Soltero et al. 1974), Lake Powell, Utah-Arizona (Johnson and Merritt 1979), and Lake Kootenay, British Columbia (Hamblin and Carmack 1978, Carmack 1979), among others.

14. Serruya (1974) described the inflow into Lake Kinneret, Israel, using conductivity data. This was an excellent example of inflow into a wide body of water. It also illustrated the effects of Coriolis accelerations which caused the density interfaces to tilt to the right side (looking downstream) of the basin, as expected in the northern hemisphere. Hamblin and Carmack (1978) have analyzed these types of flow in detail.

15. Hebbert et al. (1979) studied a saline underflow into Wellington Reservoir, Australia, where the flushing of salts from the watershed caused salinity concentrations to peak before flow. The authors showed that both the flood and salinity surges travelled at constant speeds but that the flood surge travelled 2.3 times faster than the salinity surge and therefore moved past the salinity surge in the reservoir.

16. Perhaps the most complete set of data describing turbid inflows into a reservoir has been collected by J. Nix and staff, Ouachita Baptist University, on DeGray Lake, Arkansas. Observations included overflows, interflows, and underflows during both base and elevated flow regimes. Inflows were tracked using turbidity, calcium, and specific conductance. These density currents are discussed in part by Thornton et al. (1980), Ford et al. (1980), Ford and Johnson (1981), and Nix (1981) and completely documented by Johnson et al. (1983).

Dye studies

17. When there is no naturally occurring property which can be easily detected and measured, inflows can be labeled with an artificial tracer to follow their behavior. Fluorescent dyes have proven to be excellent tracers because of their properties of high detectability and ease of handling. Johnson (1983) discusses fluorescent dyes and their use.

18. A number of field studies using fluorescent dyes have been performed. Many of these studies have not been fully documented or published in a form that is readily available, thus, the following discussion is not complete.

19. One of the first dye studies documented was by Elder and Wunderlich (1968). They dyed the Nantahala River flowing into Fontana Reservoir, Tennessee, using Rhodamine B fluorescent dye. The dye flowed through the reservoir as an interflow and travelled approximately 32 km in a period of 6 weeks (approximately 0.9 cm/s) before becoming undetectable. As the reservoir elevation dropped, the dye also sank to a lower elevation but remained well-defined indicating that little or no mixing occurred. Since the inflow temperature varied by over 2°C during dye injection, it was suspected that the dye moved into different layers, creating the appearance of vertical mixing or diffusion.

20. Bayne (1967) studied the movement and dispersion of the Chattahoochee River as it moved through Lake Eufaula, Alabama, using Rhodamine WT fluorescent dye. In the upper reaches of the reservoir, the water movement was riverlike with an average velocity of 0.13 m/s. In the middle section, the dye moved as an underflow following the old river channel with an average speed of 0.04 m/s. In the lower end of the reservoir, the dye movement was erratic and was even observed to move upstream. This may have been caused by a constriction in an earthen causeway.

21. Morris and Thackston (1969) used two dye injections to study the movement of the South and North Forks of the Holston River through Cherokee Reservoir, Tennessee. In the first dye study, a cold-water pulse from the South Fork was dyed; in the second study, the warmer North Fork was dyed. Both inflows moved through the reservoir as interflows; during the second study, the interflow was thicker and proceeded at a greater depth because stratification was weaker. In both studies, the dye was well-mixed laterally. During a period of slow continuous drawdown, no dye was observed to move into the coves. Some horizontal movement of dye into the coves was observed when the water surface fluctuated by up to 0.12 m. Virtually no vertical transport was observed.

22. Chasse and Slotta (1972) made 12 dye releases into three reservoirs (Hills Creek, Cougar, and Dorena) in Oregon. Although most

of the studies were on Hills Creek Reservoir; a wide range of conditions was studied. Both interflows and underflows were observed; current thicknesses varied from 3 to 12 m; current speeds varied from 0.02 to 0.15 m/s. Chasse and Slotta also computed entrainment rates, which varied from 1.00 (no entrainment) to 4.0 (300% entrainment). In Cougar Reservoir, the dye entered at two elevations; no explanation was given for the formation of two distinct interflows.

23. Sutron Corporation (1980) studied the lateral mixing characteristics in Lewis and Clark Lake, South Dakota, on the Missouri River. Rhodamine WT fluorescent dye was injected into the river above the lake and followed through the lake. In the upper reaches of the lake, the dye remained in the zone of maximum velocity. In the main body of the lake, wind appeared to influence the movement of the dye. The dye was not well-mixed laterally at any time. A two-dimensional transport model was used to investigate lateral mixing and the influence of the wind.

24. Fischer and Smith (1982) studied an underflow in the Las Vegas arm of Lake Mead. Rhodamine WT dye was used to determine the movement of inflowing nutrients into the water surface. The study demonstrated that the nutrients (dye) reached the surface through the current field generated by large internal waves (as high as 6 m) and the transient formation and destruction of secondary thermoclines due to variations in meteorological conditions.

25. Ford et al. (1980) also documented the effects of variations in meteorological conditions on inflow currents. Convective mixing at night divided a dye cloud into three distinct parts. This study and others on DeGray Lake, described by Johnson et al. (1983), showed that even under low-flow conditions, density currents move through lakes in distinct layers.

Complicating Factors

26. Based on the field observations, there are a number of factors which complicate the analysis and prediction of density currents in reservoirs. These include complicated morphometry, unsteady and

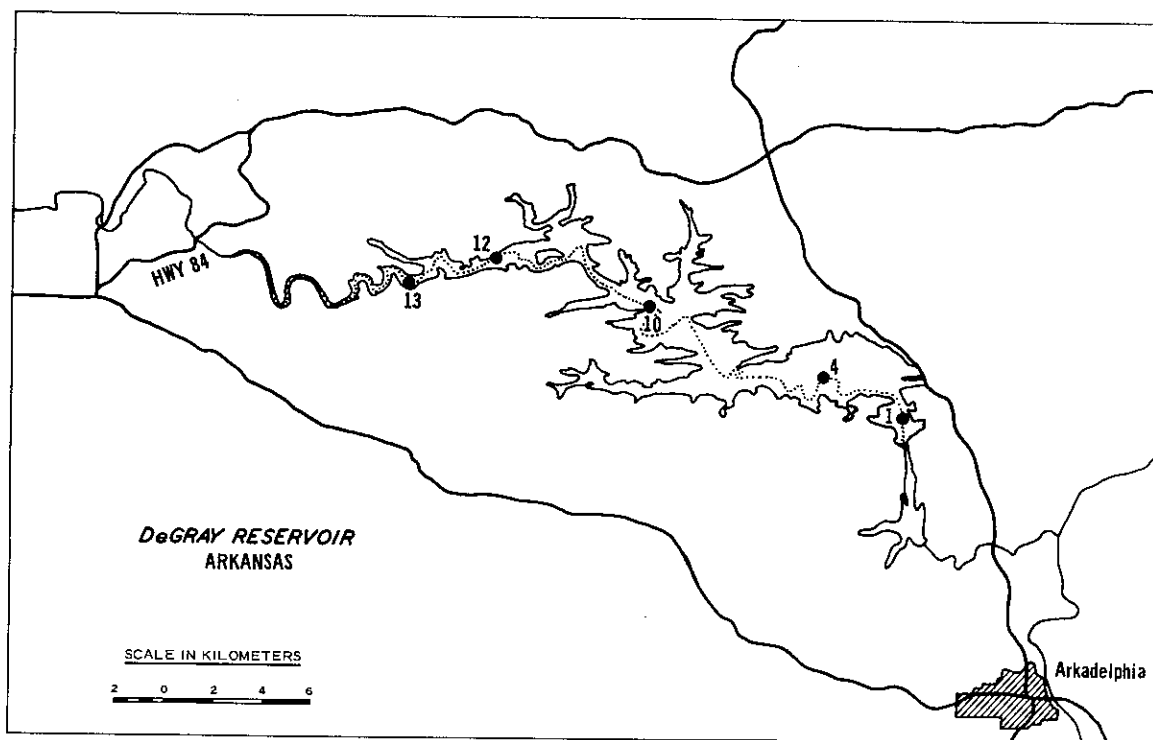


Figure 4. Typical long, dendritic reservoir with meandering thalweg.

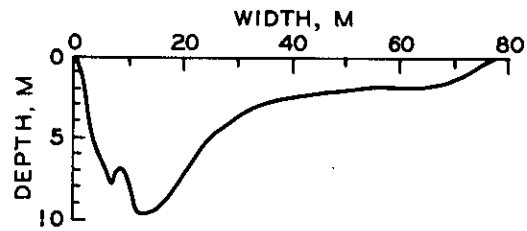
multiple tributary inflows, variable stratification, and man-made perturbations and constraints.

Complicated morphometry

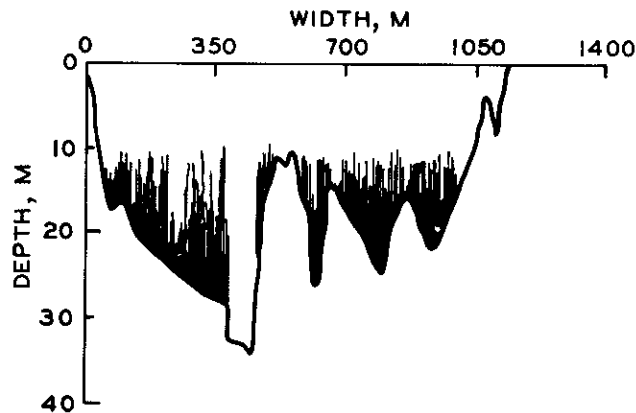
27. Reservoirs are typically built in deep valleys downstream of the confluence of several tributaries. The resulting lake is long, highly dendritic, and possibly surrounded by high terrain (e.g. Figure 4). The many coves, embayments, and islands make the width highly variable and difficult to define. Field observations of turbidity currents in DeGray Lake, Arkansas, (Ford and Johnson 1981) indicated that in many instances, density currents were not well-mixed laterally but followed the thalweg of the inundated river (Figure 5). This phenomenon has also been observed in other reservoirs (e.g. Lake Red Rock, Iowa, Lewis and Clark Lake, South Dakota). In many cases, especially in reservoirs that have not been cleared of trees, the zone above the old channel may be the path of least resistance. Sonar recordings from



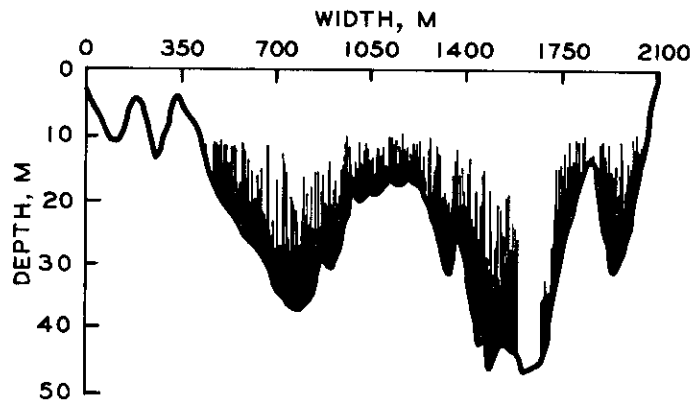
Figure 5. Turbid inflow to DeGray Lake following thalweg.



a. Upstream of Station 12



b. Downstream of Station 10



c. Near Station 4

Figure 6. Typical cross sections from DeGray Lake
(See Figure 4 for station locations).

three typical cross sections of DeGray Lake are shown in Figure 6. Upstream of Station 12, all of the trees have been removed and the cross section is typical of a free-flowing river (Figure 6a).

Downstream of Station 10, the trees were topped at elevation 113 m above mean sea level (msl), or approximately 11 m below normal pool elevation (Figure 6b), an elevation within the metalimnion during the summer stratification. The cross section shown in Figure 6c is located near Station 4. The old river channel is well-defined in all three cross sections. Density flows occurring at elevations below the tree level were constrained to the old river channel; many of the interflows occurred at elevations near or slightly above the tree tops.

28. Since density currents may not be well-mixed laterally, it may be necessary to define the width or limits for the zone of conveyance. The appropriate width and length scales for density currents may be the width and length of the old river channel, respectively.

29. Old roadways, railroad crossings, etc., that were not removed prior to the filling of a reservoir may also act as hydraulic controls to direct the density current. For example, in Lake Red Rock the embankment for a low-water bridge was not removed (Figure 7). This embankment, which is submerged at flood pool, acts as a barrier to direct flow along the south shore. Old cofferdams, construction roads, etc., are also sometimes inundated causing perturbations and irregularities in the anticipated flow field. If an old roadway extends across the reservoir, the density current may buildup behind the roadway prior to flowing over it (Knapp 1942).

30. The slope of old river channel may be modified due to sedimentation and changes in the configuration of the delta region. In Lake Red Rock, over 6 m of sedimentation occurred in the old river channel during the first seven years of operation (Kennedy et al. 1981). The path of the channel through the delta also changed several times. In Lake Mead, Nevada-Arizona, the delta progressed 67 km in 13 years (Vanoni 1975).

Unsteady and multiple inflows

31. The magnitude and timing of tributary inflows to reservoirs is dependent on the size and shape of the watershed, antecedent conditions, and the distribution of precipitation. In northern latitudes, runoff



Figure 7. Aerial photograph of Lake Red Rock, IA, showing old low-water bridge and delta formation.

from the spring snowmelt may dominate the water budget; elsewhere, the water budget may be dominated by individual storm events (e.g., see Figure 8). In either case, the major contributions to a reservoir's water budget occur during dynamic elevated flow events and not during steady base flow conditions.

32. The density of the inflowing waters is also variable. As previously stated, water density is a function of temperature, suspended solids (SS), and total dissolved solids, (TDS). Water temperatures vary seasonally, synoptically (i.e., for periods of 5-10 days), and diurnally in response to hydrometeorological forcing (Ford and Ford 1982). SS and TDS concentrations vary with runoff, flow, antecedent conditions, and other factors. Examples of the types of variations in flow, temperature, SS, TDS, and density that can occur during a storm event are shown in Figures 9 through 11 for DeGray Lake. Flows increased from approximately $8.5 \text{ m}^3/\text{s}$ at 1200 hours on 3 May to a peak of $190 \text{ m}^3/\text{s}$ at 0700 hours on 4 May, while stream temperatures dropped from 18.2°C on 3 May to 13.8°C on 5 May. Turbidity increased on the rising limb of the hydrograph and attained a maximum of 73 NTU's 11 hours prior to the peak of the hydrograph. In contrast, specific conductance, which is proportional to TDS, decreased with increased flow. Since water density is dependent on temperature, TDS, and SS, it will also vary significantly during the storm event. As the inflow density varies during the storm, the inflow will be placed at different levels in the reservoir (Figure 12). Other storm events, described by Thornton et al. (1980), Ford and Johnson (1981), and Johnson et al. (1983), demonstrated that each storm is different and, in some cases, temperature increases during the storm (Figure 13). Runoff also can increase TDS or salinity on the rising side of the hydrograph (e.g., Hebbert et al. 1979).

33. The unique thermal-density properties of water also create some complicated inflow patterns as water warms and passes through its maximum density at 4°C . Using data from Kamloops Lake, British Columbia, Carmack (1979) found that when inflow water above 4°C enters a lake with a temperature of less than 4°C , the two waters mix creating a denser

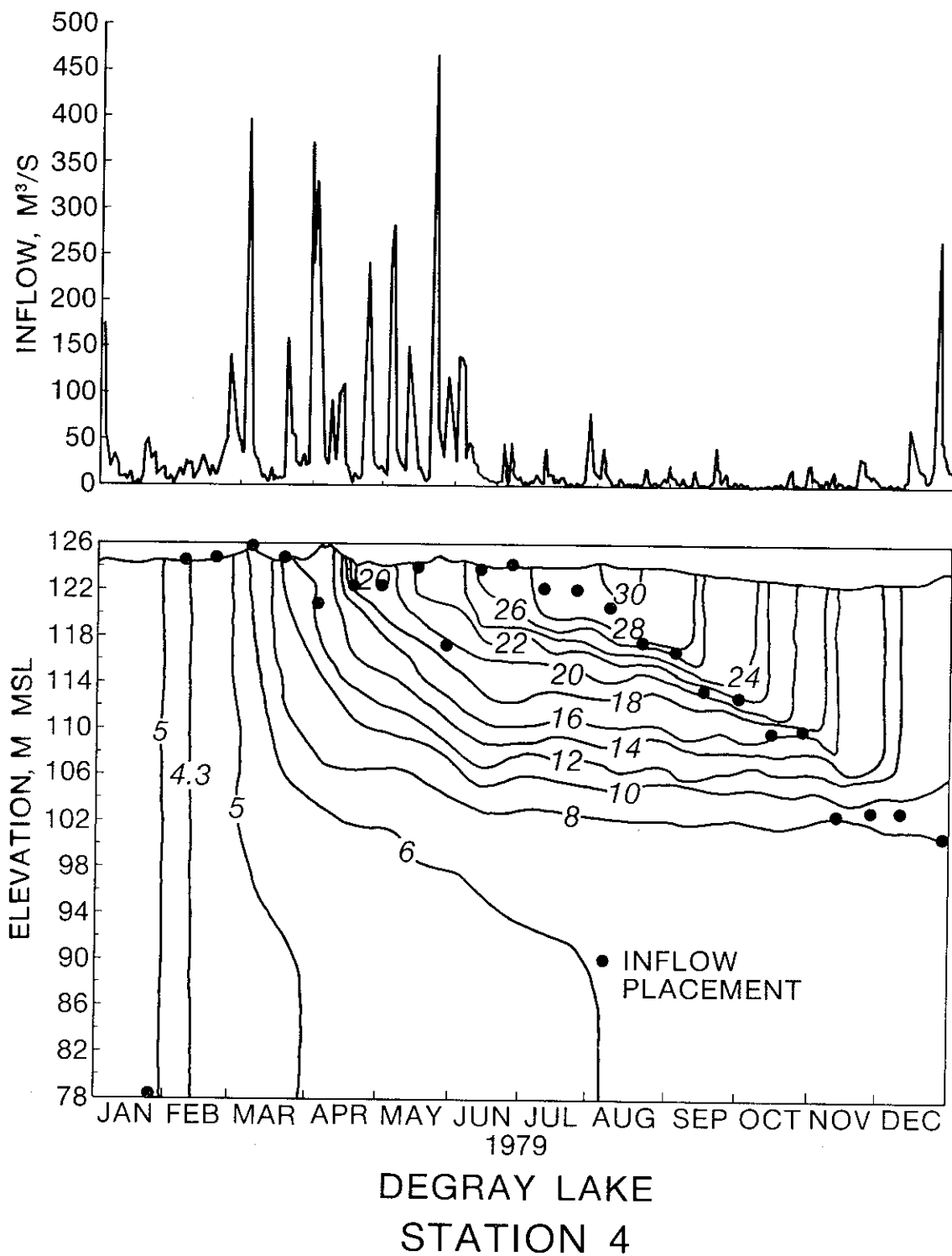


Figure 8. Inflow hydrograph and placement (isotherms are in °C).

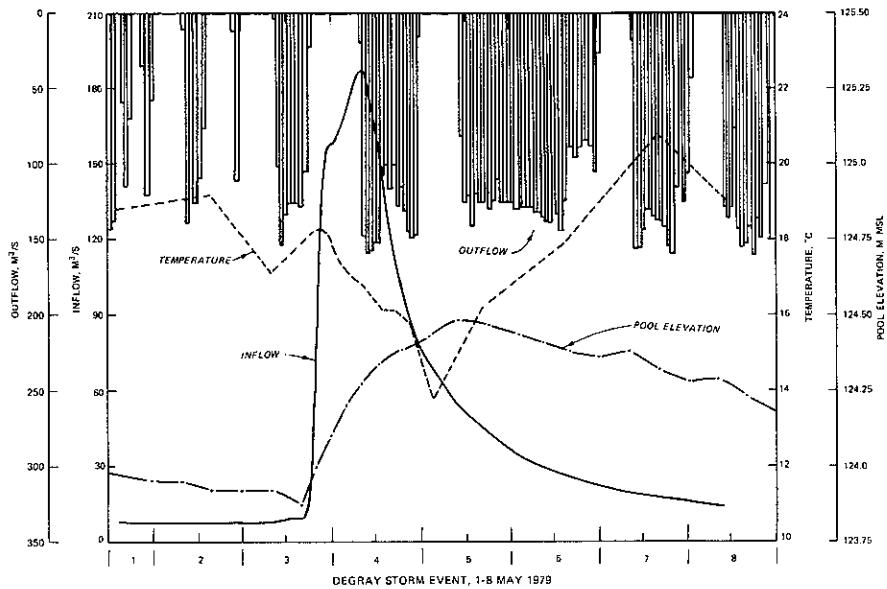


Figure 9. Inflow, inflow temperature, outflow, and pool elevation for 1-8 May 1979 storm event, Caddo River, DeGray Lake, AR.

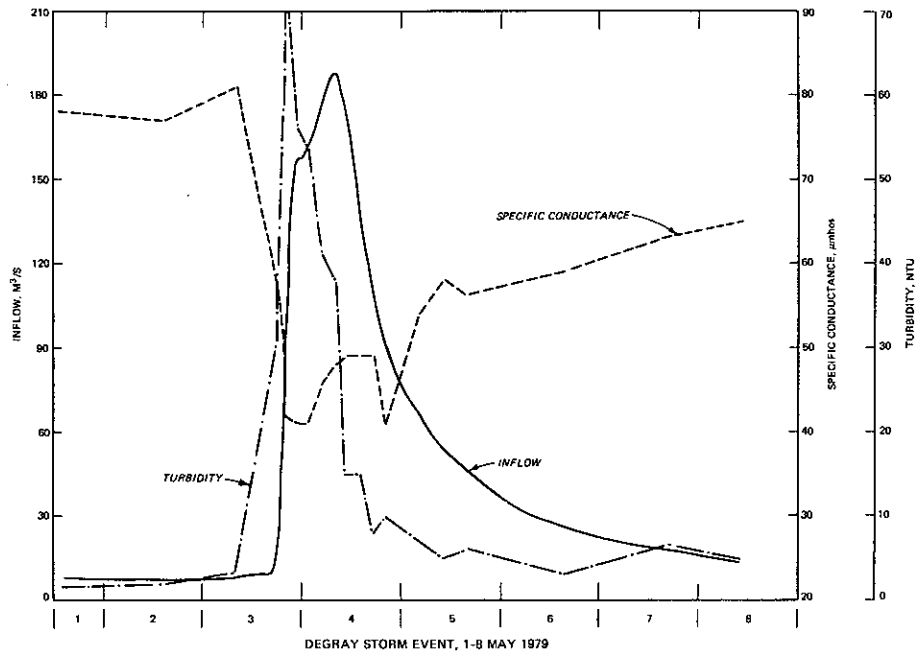


Figure 10. Temporal variation of specific conductance, inflows, and turbidity during 1-8 May 1979 storm event, Caddo River, DeGray Lake, AR.

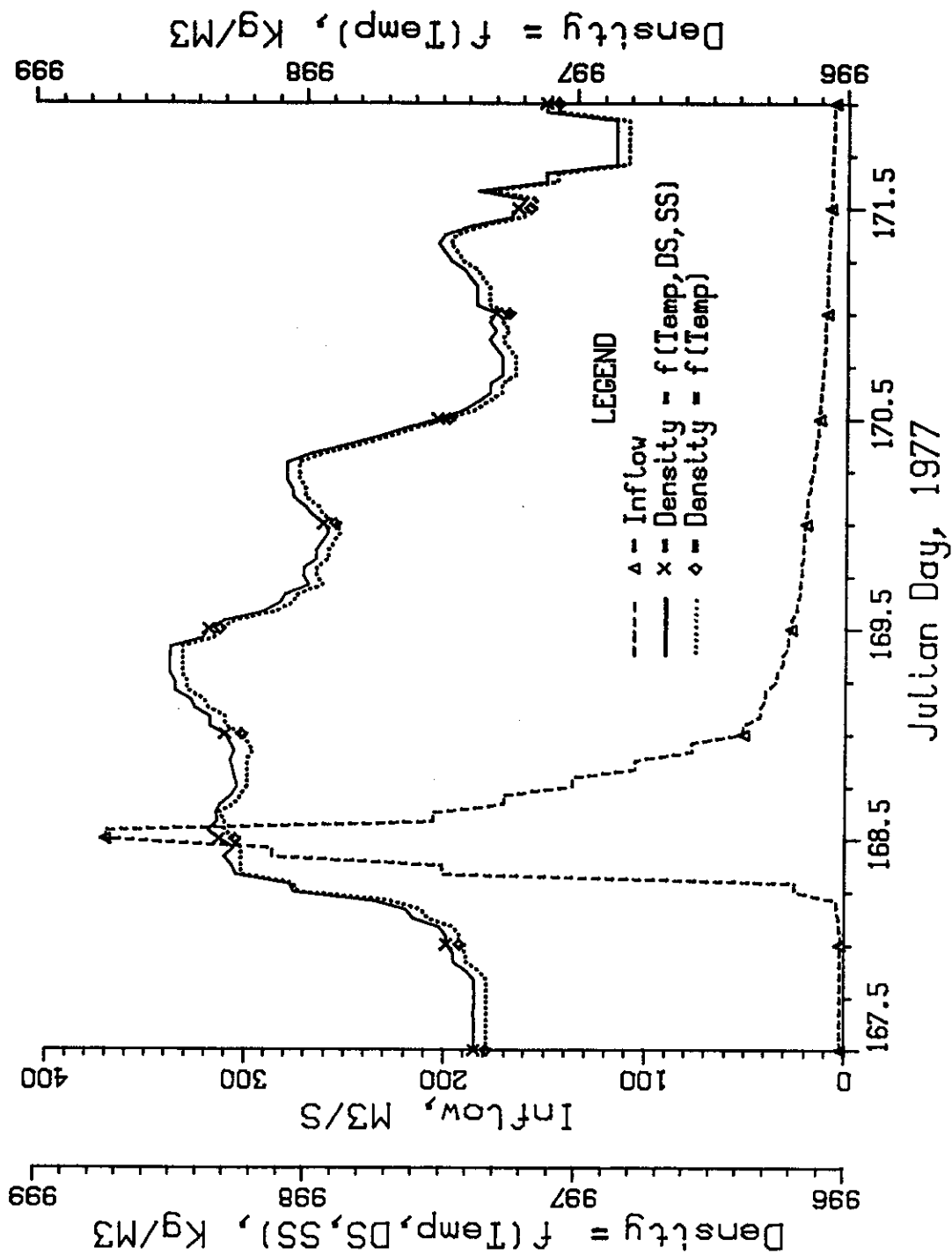
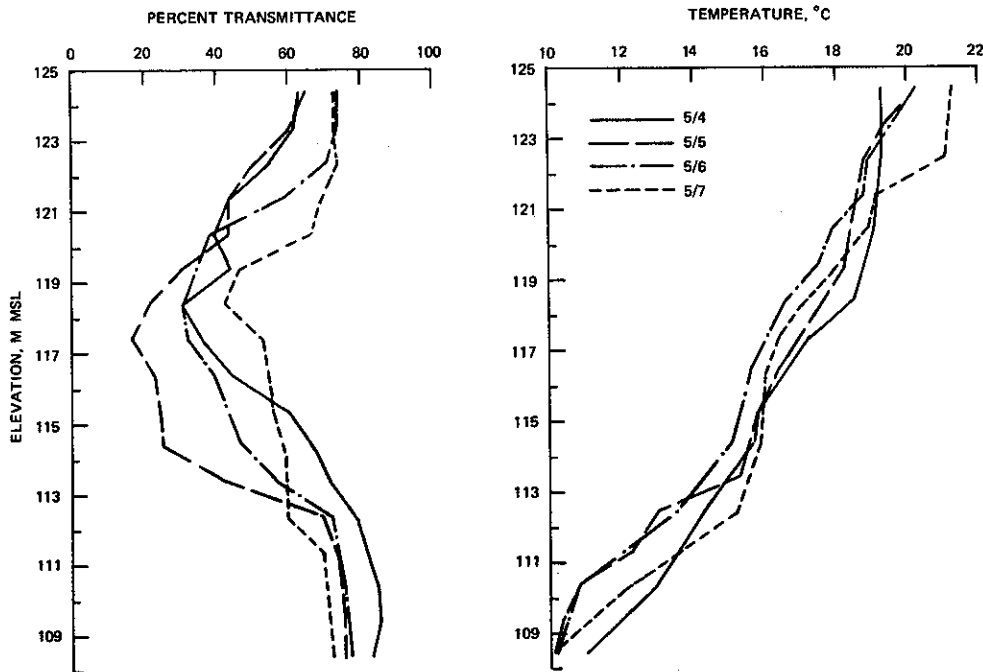


Figure 11. Temporal variation of inflow and inflow density during June 1977 storm event, Caddo River, DeGray Lake, AR.



STATION 12, MAY 1979

Figure 12. Variation in inflow placement when no mixing and entrainment are assumed, for May 1979 storm event, Caddo River, DeGray Lake, AR.

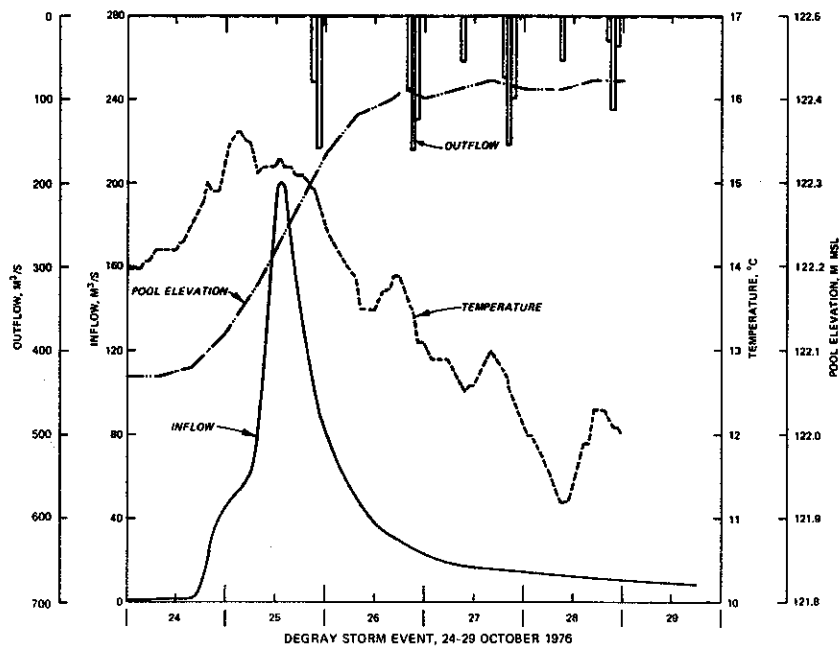


Figure 13. Increase in temperature during 24-29 October 1976 storm event, Caddo River, DeGray Lake, AR.

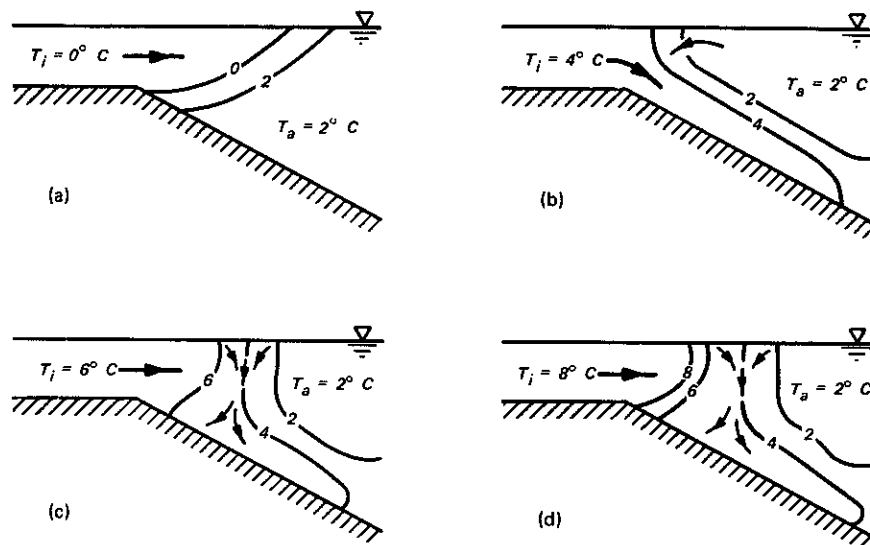


Figure 14. Inflow mixing and cabbelling as inflow temperature increases from 0°C to 8°C (after Carmack 1979).

mixture near 4°C , which sinks. This process is called cabbelling. Following Carmack (1979), a simple example which assumes a constant lake temperature of 2°C and an inflow temperature that warms from 0 to 8°C , is used to illustrate the complex circulation patterns which can develop (Figure 14). In Figure 14a, the inflowing water at a temperature of 0°C is less dense than the lake water at 2°C and the inflow enters as an overflow. In Figure 14b, the inflow is more dense and enters the lake as an underflow. When the river temperature is 6°C , it mixes with the 2°C lake water to form a mixture which is more dense and sinks (Figure 14c). If the river temperature is 8°C , it may form a mixture with the lake water (a) in the range of 2 to 6°C which would sink and create mixing or (b) in the range of 6 to 8°C , in which case the inflow would continue to float on the water surface.

34. Instabilities in the inflow current can also occur when water density is dependent on SS and TDS concentrations. As velocities decrease when the current enters a reservoir, SS will settle out thereby changing the water density. Since dissolved salts and temperature diffuse at different rates (molecular diffusivity of heat is greater

than that of salt) instabilities can also occur which increase mixing. This process is called double diffusion and is described by Turner (1973).

35. When multiple tributaries enter a reservoir, they may move through as distinct currents or they may interact to form a common current. Koryak et al. (1979) found two distinct currents in Tygart River Lake, West Virginia. The smaller, cooler tributary flowed through the lake as a distinct interflow at a deeper stratum. In West Point Reservoir, Georgia, the warmer, clearer waters of Yellow Jacket Creek appear to flow over the heavier, sediment-laden waters of the Chat-tahoochee River (Kennedy et al. 1982). The interactions between these two tributaries are highly complex.

Variable Stratification

36. As with the tributary inflows, the in-lake stratification also varies in response to hydrometeorologic forcing, but not at the same rate. The larger volume of water in the lake responds at a slower rate than the river water. During the spring, the river water warms at a faster rate than the lake water; in the fall, river water cools at a faster rate than the lake water. This is why overflows typically occur in the spring and interflows and underflows occur in late summer and fall (Figure 8).

37. An example of changes in stratification occurring during a storm event at DeGray Lake is shown in Figure 15. An intrusion entered the reservoir at an elevation of 116.5 m msl, or at a temperature of 20°C as indicated by the intersection of the temperature profiles in Figure 15. On 18 June, the temperature stratification was altered due to the intrusion. The turbidity and temperature profiles for that day indicated that the intrusion cooled the water above and warmed the water below the entrance elevation. By 19 June, the water that was warmed below the center-line elevation had returned to its previous temperature, indicating that the stratification was only temporarily displaced on 18 June and that no significant mixing had occurred. In contrast, the stratification above the center-line elevation was permanently altered,

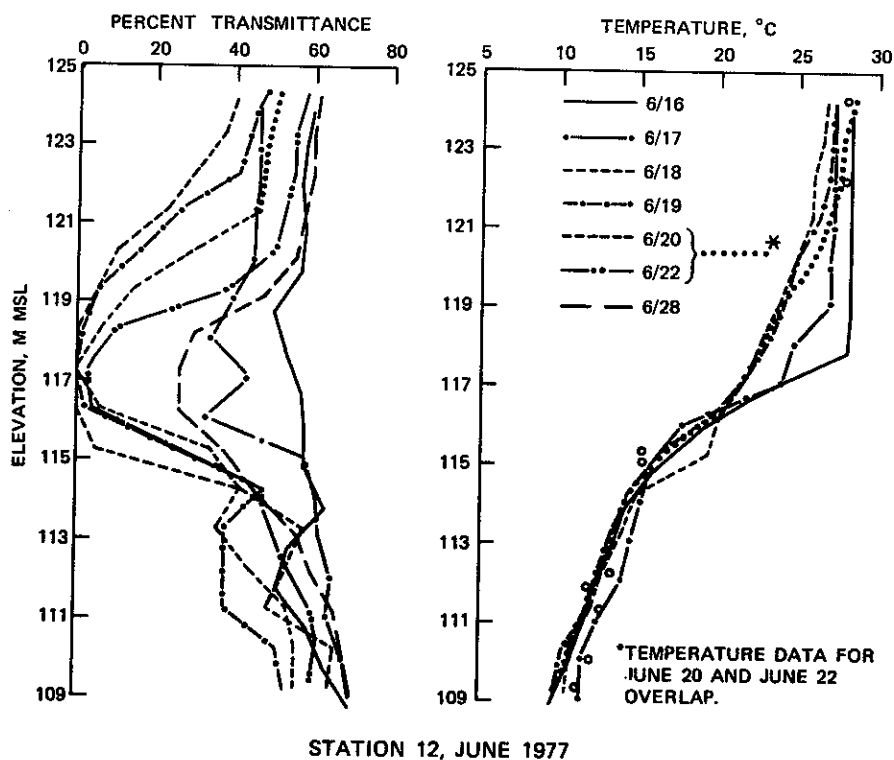


Figure 15. Variations in thermal stratification during June 1977 storm event, DeGray Lake, AR.

indicating mixing. This mixing was probably due to a shear mechanism. After 19 June, the temperature profiles showed that surface mixing dominated.

38. Surface mixing phenomena were observed to dominate during a dye study on DeGray Lake in 1979. Nocturnal convective mixing caused the dye cloud to break into two parts on 14 October and into three parts on 15 October (Figure 16). The origin of these breaks can be traced back to the locations at kilometers 2.8 and 4.0 where a greater volume of water from deep holes and embayments was available for mixing and dilution of the dye cloud at night. This convective mixing contributed to the increased diffusion coefficient. It was only after the weather had warmed and the reservoir had restratified that the classical underflow was observed on 17 October.

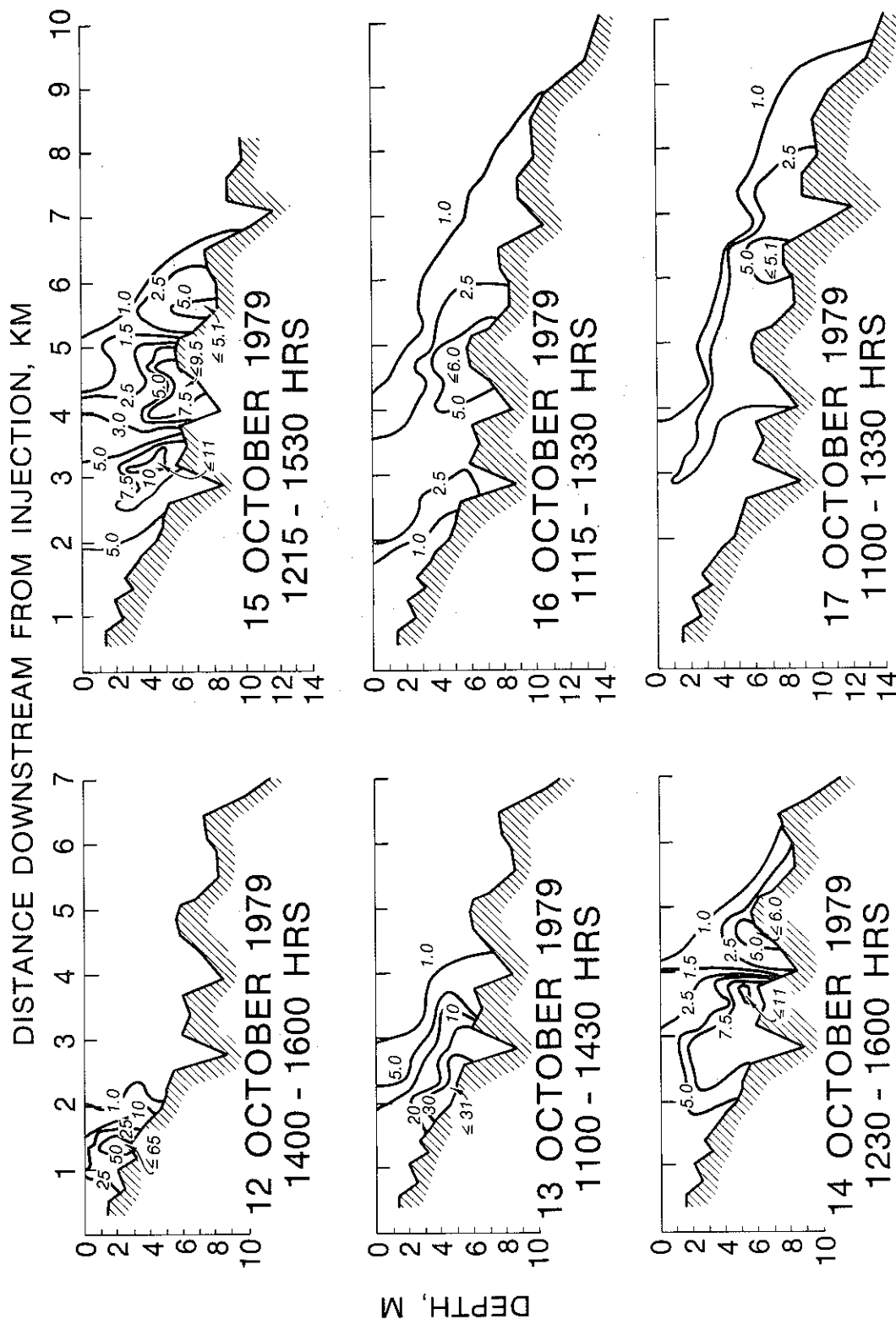


Figure 16. Nocturnal mixing during October 1979 dye study, DeGray Lake, AR (isopleths in ppb).

Man-made perturbations and constraints

39. Project operation and point source discharges also can modify the behavior of density currents. Many reservoirs are characterized by wide fluctuations in pool elevation. Water is stored during periods of high flow and released during periods of low flow. In hydropower projects, releases are made only to generate power. In either case, whenever a project is operated such that inflow is not equal to outflow, density currents are governed by unsteady forces making their analyses difficult. For example, Ford and Johnson (1981) showed that a density flow stalled and collapsed in DeGray Lake when the outflows were stopped. In both the May 1979 storm (Figure 9) and October 1976 storm (Figure 13), the lake surface rose since the inflow was greater than the outflow. This caused water to move back into the coves, complicating the analysis of the density current.

40. The level of the withdrawal is also important. Bottom withdrawal projects reinforce the movement of underflows. Withdrawing water from a level different from that of the density current can generate secondary currents which complicate the analysis.

Water Quality Implications

41. Inflows to impoundments not only contribute to the water budget but also carry solids, nutrients, bacteria, and other substances that affect reservoir water quality. These materials may enter the epilimnion, metalimnion, or hypolimnion depending on whether an overflow, interflow, or underflow occurs. If an overflow occurs, the nutrients enter the epilimnion directly and are immediately available for phytoplankton uptake. Coliform bacteria entering the epilimnion may impact body-contact recreation in the upper reaches of a reservoir (Thornton, et al. 1980). If an interflow or underflow occurs, the transported materials will plunge below the water surface and may pass through the reservoir at a level that would not impact the surface waters. Fischer and Smith (1982) showed that it is still possible for inflowing nutrients to get to the surface waters by various mixing mechanisms even

though a well defined interflow existed. A cold inflow, rich in dissolved oxygen, may also find its way into an anaerobic hypolimnion, allowing oxidation of substances there. Koryak et al. (1979) showed that interflows in Tygart River Lake, West Virginia, helped to mitigate the effects of acid mine drainage.

42. Recent studies have shown that significantly more material enters a reservoir during storm events than during base flow conditions (Perrier et al. 1977, Westerdahl et al. 1981). During storms, certain constituents (e.g., phosphorus, coliform bacteria, turbidity) characteristically load on the rising side of the hydrograph while others (e.g., nitrate and many metals) load on the falling limb (Perrier et al. 1977, Westerdahl et al. 1981). The ultimate fate of a constituent will depend not only on how it moves through the reservoir but also on how it loads on the hydrograph. Using the two-dimensional model LARM, Johnson et al. (1981) showed that turbidity, fecal coliforms, nitrogen, and phosphorus moved through DeGray Lake at different rates and elevations depending on the unique manner in which each constituent loaded on the hydrograph.

43. Density currents can also produce flow reversals in the reservoir that cause undesirable materials to be transported upstream. When the cool inflow plunges beneath the surface and enters the reservoir as an interflow or as an underflow, some of the reservoir water is entrained and a counteracting circulation pattern is set up in the overlying surface waters. This reverse flow pattern transports floating debris upstream to the plunge point where it remains at the surface. Water is again entrained and plunges to continue the circular pattern. Bell (1942) noted that in June 1941 a driftwood barrier was set up in Lake Mead, Nevada-Arizona, in this manner from bank to bank, extending several thousand feet long and effectively blocking all navigation.

44. Another problem associated with induced flow reversal occurs when municipal water intakes are located upstream of waste discharges. Fry et al. (1953) reported two such cases for the cities of Harriman and Knoxville, Tennessee. Knoxville's water intakes are located just

inside the upstream limit of Fort Loudin Reservoir's pool, upstream of sewage and industrial waste outfalls. A TVA study determined that, unless the tributary inflows to the reservoir filled the entire river-like channel in the reservoir near the intakes, the inflow would plunge and become an underflow. Then, as the underflow moved downstream, the resulting return current above it would transport sewage and industrial wastes upstream to Knoxville's water intakes. To prevent such an occurrence, minimum release criteria were established for the two upstream reservoirs supplying the cold tributary inflows to Fort Loudin Reservoir.

45. At Harriman a more complicated situation existed. Harriman's water intakes were located in the Emory River arm of Watts Bar Reservoir upstream of sewage and paper mill discharges. Density currents in the Clinch River arm of the reservoir often traveled downstream into a pool connecting both arms and then upstream into the Emory River arm. The invasion of a density current into the Emory River arm itself posed no hazard to Harriman. A problem was created, however, when the intruding density current stalled and began moving back downstream the Emory River arm as a result of reductions in outflows from the upstream reservoir feeding the density current. As the density current moved back downstream, downstream water moved upstream to replace it, transporting the sewage and paper mill effluent upstream to Harriman's water intakes. The city of Harriman was eventually forced to move their water intakes further upstream in the Emory River arm of the reservoir, beyond the influence of invading density currents.

46. Recent research on reservoir limnology emphasizes the development and maintenance of longitudinal gradients in reservoirs. To explain these gradients, Thornton et al. (1981) have proposed a heuristic model which divides a reservoir into a riverine zone, transition zone, and lacustrine zone (Figure 17). The definition of these zones is dependent on how reservoir inflows enter and move through reservoirs. In the riverine zone, current velocities are decreasing but the advective forces are still sufficient to maintain a well-mixed environment. In

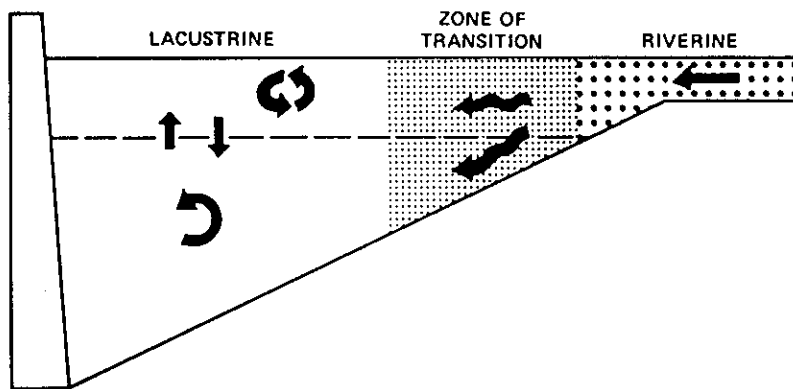


Figure 17. Riverine, transitional, and lacustrine zones in a reservoir (after Thornton et al. 1981).

the transition zone, the buoyancy forces begin to dominate over the advective forces and the inflow plunges. The upstream and downstream boundaries of the transition zone may correspond with the location of the plunge point under low-flow and high-flow conditions, respectively; this zone is also the zone of sedimentation. In the lacustrine zone, buoyancy forces dominate and inflows move through the reservoir in well-defined horizontal layers as interflows and underflows.

Discussion

47. The literature review indicates that an understanding of reservoir density currents and inflow mixing processes is essential to understanding reservoir water quality, especially with respect to the importance of storm events. The review also indicates that the analysis of density currents requires an in-depth knowledge of inflow characteristics, ambient reservoir conditions, and reservoir geometry. It is therefore important to review these factors prior to evaluating predictive techniques for density currents.

48. The important attributes of inflow are flow rate and density. Both are highly variable. Although inflows to many CE reservoirs are gaged or easily back-calculated from outflows and changes in

storage, it is the inflow momentum, rather than the total discharge, that is important when analyzing inflow density currents. The inflow momentum is usually difficult to assess and may not be directly related to the total inflow rate, since it varies as the width and thickness of the flow zone change. The inflow density is a function of temperature, TDS, and SS. Inflow temperatures vary with hydrometeorological conditions and are easily measured or computed from heat budget considerations (Ford and Ford 1982). TDS concentrations can increase or decrease with flow and are usually related to specific conductance, which is easily measured. SS concentrations can sometimes be correlated with flow, but their density contribution is complicated by settling and deposition as the inflow enters a reservoir. Although the inflow characteristics of flow rate and density are both measurable and predictable, the quantification of inflow momentum and SS concentrations is not a simple task.

49. The ambient reservoir conditions that are important for density current analysis include density stratification, current structure, and turbulence levels. Ambient reservoir conditions are also highly dynamic but, with the exception of temperature, they are neither easily measured nor predicted. The internal current structure and turbulence level depend on such ungovernable factors as wind speed, variability, and direction, and on such project operation factors as discharge rate and withdrawal depth.

50. Irregular reservoir geometry also complicates the analysis of density currents since widths, depths, and cross-sectional areas do not vary uniformly. The characteristic dendritic shape of reservoirs usually indicates that more than one tributary enters the reservoir at different locations and that the many coves and embayments may be isolated and not part of the zone of conveyance. In addition, islands may produce the bifurcation of an inflow density current. Other factors that influence the movement of density currents and must therefore be considered are bottom roughness caused by uncut timber, for example, and man-made obstacles such as low-water bridges, earthen embankments, and cofferdams.

51. In summary, when evaluating predictive techniques for reservoir density currents, one must realize that assumptions such as uniform flow, steady state, constant width, constant density, and two-layered systems are not representative of actual conditions.

PART III: PREDICTIVE TECHNIQUES

52. Numerous simplified techniques have been proposed in the literature to predict the characteristics of density currents. These are reviewed and evaluated in this section using field data collected from a number of sources including Johnson et al. 1983 and Kennedy et al. 1983. The predictive techniques for overflows, plunge point location, initial mixing and entrainment, underflows, and intrusions or interflows are discussed. Use of the equations recommended for predicting plunge point location, initial mixing, interflow thickness, and propagation speed is demonstrated in Appendix B, employing examples from DeGray Lake, Arkansas. Appendix C outlines an inflow algorithm for predicting inflow placement, plunge point depth, initial mixing, underflow entrainment, and intrusion thickness, which is to be used in a one-dimensional water quality model such as CE-QUAL-R1 (Environmental Laboratory 1982).

Overflows

53. Whenever inflowing water is less dense than the surface water of the reservoir, the inflowing water will float on the water surface and an overflow occurs. Several problems analogous to a density overflow have been studied intensively. These include thermal discharges (e.g., Adams et al. 1975, Safaie 1979, Harleman 1975) and oil slicks (e.g., Wilkinson 1972, 1973). In addition, Kao (1977) showed that a dense front penetrating into an infinitely deep layer of lighter fluid is analogous to an overflow situation.

54. Three factors must be considered when analyzing overflows; these are: the separation or lift-off point, the extent of horizontal spreading, and the propagation speed.

Separation point

55. The separation or lift-off point is that point where the buoyancy forces exceed the advective forces and the inflowing water floats on the water surface (Figure 1). The separation point is

analogous to the plunge point; relationships for the plunge point should also be valid for the separation point (see next section on plunge points).

56. In a series of laboratory experiments using a point discharge into a wide tank over a sloping bottom, Safaie (1979) found the following empirical equation for the separation depth h_p^* :

$$h_p = 0.914h_i(F_i)^{1/2} \quad (1)$$

where

h_p = separation depth

h_i = inflow depth

and the inflow Froude number:

$$F_i = \left(\frac{u_i}{\left(\frac{\Delta\rho_i g h_i}{\rho_a} \right)^{1/2}} \right)^{1/2} \quad (2)$$

where

u_i = inflow velocity

ρ_a = density of receiving water

ρ_i = density of inflowing water

$\Delta\rho_i = (\rho_a - \rho_i)$ = density difference between receiving water and inflow

g = gravitational acceleration

Equation (1) predicted separation depths which agreed well with laboratory experiments ($R^2 = 0.93$) and was verified against data from other

* Symbols used in this report are defined once where used in the main text and appendices and, for convenience, are listed and redefined in Appendix D. Unless specifically stated, all equations presented in this report are dimensionally consistent, and either metric (SI) or U. S. Customary units can be used provided the user is consistent in the application.

investigations and field studies on thermal discharges. Equation (1) is valid for $F_i > 1.2$. If $F_i < 1.2$, then $h_p < h_i$ indicating the point of separation moves up into the inflowing river like a salt wedge in an estuary. This result is consistent with the work of Stigebrandt (1978). Under these circumstances (i.e. $F_i < 1.2$), the separation point can be assumed to occur at the upper end of the reservoir.

Horizontal spreading

57. The extent of horizontal spreading is also dependent on the inflow Froude number, F_i . Safaie (1979) found that for $F_i < 3$, the flow was mainly an unsteady buoyancy-driven spread of warm water over the water surface in all directions. Therefore, for $F_i < 3$, it can be assumed that an overflow will be well-mixed laterally for all but the most abrupt entrance geometry. For $F_i > 3$, the initial spreading was controlled by the jet momentum and discharge characteristics. In jets, the outer boundaries, regardless of their definition, expand proportionally with distance, i.e.,

$$W_x = W_o + \alpha x \quad (3)$$

where

W_x = width at distance x

W_o = initial width

x = distance from source

α = 0.16 from laboratory experiments for plane jets (Fischer et al. 1979)

For shallow bodies of water, bottom interface may cause greater spreading than predicted from Equation (3). This situation will probably not occur in most reservoirs.

Propagation speed

58. Kao (1976, 1977) showed that a dense front penetrating into a infinitely deep layer of lighter fluid is analogous to an overflow situation; since this problem has been studied extensively it will be examined first. Von Karman (1940) was the first to derive an expression

for the steady propagation velocity of a dense front into a quiescent lighter fluid. Assuming a perfect fluid and irrotational flow, von Karman used Bernoulli's equation and the hydrostatic relationship to obtain

$$u_s = \sqrt{2 g h_s \frac{\Delta \rho_i}{\rho_a}} = 1.41 \sqrt{g h_s \frac{\Delta \rho_i}{\rho_a}} \quad (4)$$

where

u_s = propagation speed of the front

h_s = thickness of the underflowing current

59. Benjamin (1968) showed von Karman's reasoning was incorrect because a breaking headwave (Figure 18) was necessary to balance forces for steady propagation. Without the breaking headwave, the excess flow force per unit width,

$$\frac{1}{2} \frac{\Delta \rho_i}{\rho_a} g h_s^2$$

due to an excess in hydrostatic pressure cannot be balanced. A drag force (i.e. form drag) due to the velocity deficit in the wake region

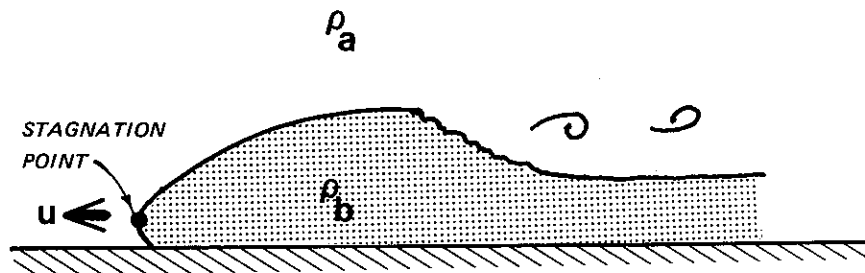


Figure 18. Breaking headwave as a heavier fluid intrudes into a lighter ambient fluid.

behind the head wave must be considered. Benjamin rederived the propagation speed as a function of relative depths and densities, showing that von Karman's result, Equation (4), is approached when the ambient fluid becomes infinitely deep.

60. The speed at which a dense front propagates into a lighter homogeneous fluid along a solid boundary has been studied in numerous laboratory experiments (Keulegan 1957, Middleton 1966, and Wood 1966, among others). In all cases, the coefficient C in the equation

$$u_s = C \sqrt{g h_s \frac{\Delta \rho_i}{\rho_a}} \quad (5)$$

was found to be less than the theoretical value of 1.41 (See Equation 4). In a review of these experiments, Benjamin (1968) found that the typical value for C was approximately 1.1. According to Benjamin, this reduced value results from a modified piezometric pressure at the stagnation point, which in practice is not located at the boundary as assumed with inviscid theory, but is located a small distance up from the boundary (Figure 18).

61. Laboratory experiments have also shown that stratification in the ambient fluid decreases the size of the head (Wilkinson and Wood 1972) which explains why density heads are not always observed in atmospheric flows and lakes. In addition, Middleton (1966) found that the shape of the front remains the same for bottom slopes up to 0.06. This discovery reinforces the fact that the processes controlling the shape and movement of the front are distinct and different from the frictional forces that control the uniform flow behind the head.

62. Following Benjamin (1968), Kao (1977) derived a general expression for the steady propagation speed of a nonuniform density current into a stratified ambient environment. Kao showed that (a) the effect of the ambient stratification was to increase the speed of the density current and (b) the speed of warmwater surface current was independent of mixing and depended only on the inflow Froude number; i.e.,

$$\frac{u_s}{u_i} = (2/F_i^2)^{1/3} \quad (6)$$

63. Koh (1976) analyzed the time-dependent spreading of a buoyant fluid on the surface of a heavier fluid. He assumed the shape of the spreading fluid was geometrically similar from one instant to the next, and divided the problem into three time scales: initially, there is a transient start-up period; then there is an intermediate time where the inertial forces balance the buoyancy driving forces; and finally, for large times, interfacial shear is dominant. For practical problems, the intermediate time scale is of interest, and Koh determined the following time (t) dependence for overflow length and thickness:

	$\frac{\text{length}}{t^{2/3}}$	$\frac{\text{thickness}}{t^{-2/3}}$
two-dimensional instantaneous release	t	1
two-dimensional continuous release	$t^{1/2}$	t^{-1}
axisymmetric instantaneous release	$t^{3/4}$	$t^{-1/2}$
axisymmetric continuous release		

Therefore, for the two-dimensional continuous release situation the overflow length is proportional to time t and the thickness is constant. For large times, however, Koh showed that the thickness is proportional to $t^{1/5}$ and would therefore increase indefinitely. In contrast, the continuous release axisymmetric case tends to a constant thickness for large times. The third dimension is sufficient to prevent blocking of the flow.

64. Assuming shear is small and the flow regime is governed by a balance of inertial and buoyant forces, Koh (1976) solved the two-dimensional continuous release problem and obtained:

$$u_s = \frac{L_s}{t} = \left(\frac{\frac{6}{\pi} \frac{\Delta \rho_i}{\rho_a} g q_i}{1 + \frac{3}{2} C_p} \right)^{1/3} \quad (7)$$

where

L_s = overflow length

q_i = unit width discharge

C_p = coefficient to account for nonhydrostatic pressure distribution

Using $C_p = 0.5$ from laboratory experiments for a surface source, Equation (7) reduces to

$$u_s = 1.03 \left(g \frac{\Delta \rho_i}{\rho_a} q_i \right)^{1/3} \quad (8)$$

and assuming uniform flow ($q_i = u_s h_s$)

$$u_s = 1.04 \sqrt{g \frac{\Delta \rho_i}{\rho_a} h_s} \quad (9)$$

Since

$$q_i t = \frac{\pi}{4} L_s h_s$$

for an overflow shaped like one quarter of an ellipse (Koh 1976), then

$$h_s = 1.24 \left(\frac{q_i^2}{g \frac{\Delta \rho_i}{\rho_a}} \right)^{1/3} \quad (10)$$

The coefficient in Equation (9) (1.04) is similar to the value of 1.1 recommended by Benjamin (1968) (Equation 5).

Summary

65. Several factors complicate the analysis of overflows. First, three-dimensional effects must be considered. Since the motive force in an overflow is the excess hydrostatic pressure, the current will spread in any direction not obstructed by boundaries. Second, an overflow will usually result from density differences due to temperature.

This temperature difference is quickly eliminated by heat transfer at the air-water interface. Third, any wind shear can (a) direct the overflow into a cove or prevent it from moving downstream and (b) enhance horizontal dispersion. Fourth, vertical mixing resulting from wind shear and/or convective cooling can distribute the current throughout the water column.

66. The overflow speed and thickness can be estimated from Equations (9) and (10), respectively.

Plunge Point Analysis

67. If the density of the inflowing river water is greater than the surface water of the reservoir, the inflow will plunge beneath the water surface. The location of the plunge point is determined by a balance of the stream momentum (i.e., dynamic force); the pressure gradient across the interface separating the river water from the reservoir water (i.e., static force); and the resisting shear forces at the bed, interface, and water surface. Since flow changes in the vicinity of the plunge point occur over distances small compared to normal cross-section changes, the flow is rapidly varying and therefore independent of slope.

68. Singh and Shah (1971) provided an excellent description of the flow in the vicinity of a plunge point (Figure 19). The location maximum velocity gradually changes from near the water surface in a

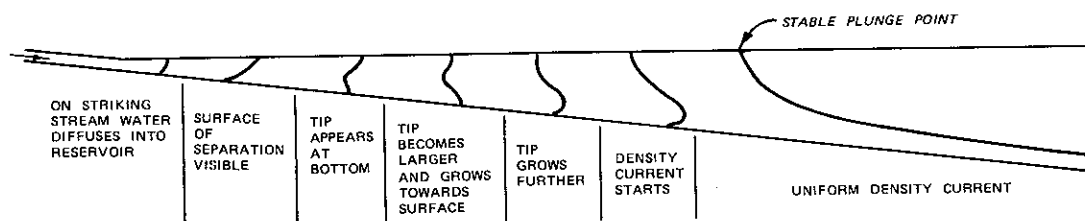


Figure 19. Flow in the vicinity of the plunge zone (after Singh and Shah 1971).

riverine zone to near the bottom in the reservoir backwater as the static force begins to dominate. At the plunge point, the flow is concentrated near the bed.

69. For small slopes and Froude numbers, under more or less steady state, the sharp line usually delineating the plunge point indicates that little mixing is occurring. However, for larger Froude numbers and unsteady conditions, mixing is probably significant and proportional to the energy loss that occurs in the vicinity of the plunge point.

70. Various investigators have proposed simple models for the plunge location (Singh and Shah 1971, Wunderlich and Elder 1973, Savage and Brimberg 1975, Hebbert et al. 1979, Jain 1981, Akiyama and Stefan 1981). Some of these have been based on experimental work (Singh and Shah 1971) and others on theoretical work (Hebbert et al. 1979, Savage and Brimberg 1975, Jain 1981, Akiyama and Stefan 1981). Assumptions vary with the investigator, but typically include steady state, constant width, no mixing, uniform velocity profiles, and constant reservoir density.

Singh and Shah

71. Singh and Shah (1971) conducted an experimental study of the plunging phenomenon using a tilting flume with salt water flowing into a reservoir filled with tap water. Using the method of least squares, Singh and Shah related the plunge point depth, h_p , to the critical depth by the equation:

$$h_p = 0.0185 + 1.3 \left(\frac{q_i^2}{g\epsilon_i} \right)^{1/3} \quad (11)$$

where

h_p = plunge point depth, m

$\epsilon_i = \Delta\rho_i/\rho_a$ = relative density difference

In this study, the unit discharge was varied from 0.5×10^{-4} to $135 \times 10^{-4} \text{ m}^2/\text{s}$, the flume slope was varied from 0.005 to 0.02, and the density difference was varied from 0.5 to 13.0 g/l. The Reynolds number ranged from 600 to 11,000. For practical applications where plunge point depths are the order of meters, the constant (0.0185), can be assumed small and Equation (11) becomes:

$$h_p = 1.3 \left(\frac{q_i^2}{g \epsilon_i} \right)^{1/3} \quad (12)$$

72. Singh and Shah also investigated the plunging phenomenon analytically. Applying the momentum principal across the transition region (Figure 20), they were able to derive an equation similar to the equation for conjugate depths of a submerged hydraulic jump. Substituting experimental values for friction, they reduced the momentum equation to:

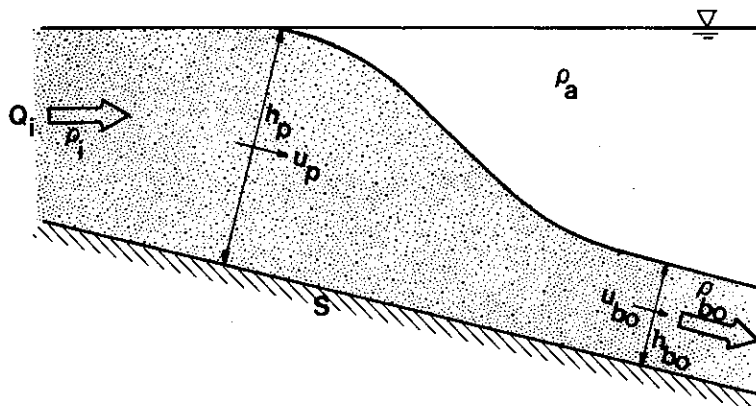


Figure 20. Schematic of plunge zone.

$$3.1 \frac{q_i^2}{g\epsilon_i} = (h_1 + h_2) (h_1 h_2)$$

where

h_1 = observed plunge depth

h_2 = thickness of underflow

Assuming h_1 is similar to h_2 ($h_1 \sim h_2 \sim h_p$), then this equation reduces to:

$$h_p = 1.16 \left(\frac{q_i^2}{g\epsilon_i} \right)^{1/3} \quad (13)$$

which is similar to Equation (12).

Wunderlich and Elder

73. Following Harleman (1961), Wunderlich and Elder (1973) assumed that conditions at the plunge point were governed by a densimetric Froude number

$$F_p = \frac{Q_i}{A} \frac{1}{(g\epsilon_i h_p)^{1/2}} \quad (14)$$

where

Q_i = discharge

$A = h_p W$ = cross-sectional area

W = width

74. Using data from the Natahala River inflow to Fontana Reservoir, Wunderlich and Elder found $F_p = 0.5$ at the plunge point. Substituting $F_p = 0.5$ into Equation (14) and rearranging terms yields the plunge point depth:

$$h_p = \frac{4.0 (Q_i/A)^2}{g\epsilon_i} \quad (15)$$

Savage and Brimberg

75. Savage and Brimberg (1975) analyzed plunging phenomena in two ways: the first was based on conservation of energy and the second on gradually varied flow theory in a two-layered stratified system.

76. In the simple energy balance, interfacial and bed friction as well as slope were neglected. The flow in the upper layer was assumed to be zero. The Froude number at the plunge point was found to be 0.5, which resulted in a plunge point depth of:

$$h_p = 1.59 \left(\frac{q_i^2}{g \epsilon_i} \right)^{1/3} \quad (16)$$

This equation was compared with the experimental data of Singh and Shah (1977) and was found to fit the data set as well as the empirical relationship (Equation 11).

77. In the two-layered analysis, Savage and Brimberg used the one-dimensional equations of motion for gradually varying flow presented by Schijf and Schönfeld (1953). These equations included bed slope and interfacial and bed friction and were used to define the shape of the interface. For the case where flow in the lower layer reaches normal depth downstream of the plunge point (i.e., an M2-type profile), the equation was integrated numerically to determine the Froude number as a function of slope and roughness. That is,

$$F_p \approx \frac{2.05}{(1+\alpha)} \left(\frac{S}{f_b} \right)^{0.478} \quad (17)$$

where

$\alpha = f_i/f_b$ = ratio of interfacial to bed friction

f_b = bed friction coefficient

f_i = interfacial friction coefficient

S = bed slope

Savage and Brimberg give ranges of 0.2 to 0.8 for α and 0.01 to 0.09

for f_b . The value for F_p can then be substituted into the equation

$$h_p = \left(\frac{q_1^2}{g \epsilon_1 F_p^2} \right)^{1/3} \quad (18)$$

to determine the plunge point depth as a function of slope and friction as well as discharge and density difference.

78. Since Singh and Shah did not present densimetric Froude numbers for their experiments, Savage and Brimberg estimated the Froude numbers to be between 0.3 and 0.8. Substitution of these limits into Equation (17) banded the data of Singh and Shah and accounted for their previous scatter.

Hebbert et al.

79. Instead of considering a rectangular cross section of unit width, Hebbert et al. (1979) considered a triangular cross section with half angle ϕ (Figure 21). Starting with the equations for conservation of volume and momentum, Hebbert et al. related the downstream normal densimetric Froude number F_n to the ratio between the downstream normal depth of flow h_n and the plunge point depth h_p (i.e., $\zeta = h_n/h_p$). The plunge point depth can then be calculated, knowing the densimetric Froude number and downstream normal depth of flow. Hebbert et al. related F_n to reservoir characteristics:

$$F_n^2 = \frac{\sin S \tan \phi}{C_D} (1 - 0.85 C_D^{1/2} \sin S) \quad (19)$$

where $C_D = (f_b + f_i)/4$ = drag coefficient.

Equation (19) states that the downstream normal densimetric Froude number is a function of reservoir characteristics only and therefore a constant for a given reservoir. The downstream normal depth of flow is then computed from

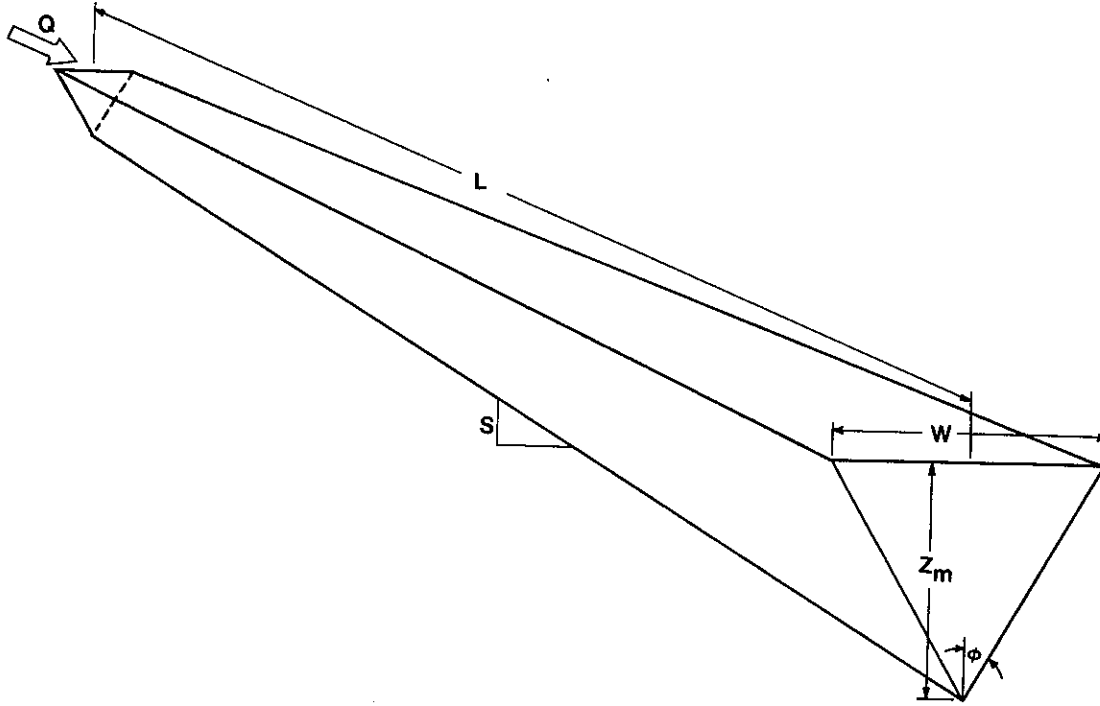


Figure 21. Triangular representation of a reservoir
(after Hebbert et al. 1979).

$$h_n = \left(\frac{2Q_i}{F_n^2 g \epsilon_i \tan^2 \phi} \right)^{1/5} \quad (20)$$

For Wellington Reservoir, Hebbert et al. found $F_n = 0.24$ and $\zeta = 0.97$ which resulted in

$$h_p = 1.16 \left(\frac{Q_i^2}{g \epsilon_i} \right)^{1/5} \quad (21)$$

For DeGray Lake, $C_D = 0.055$, $S = 1.19 \times 10^{-3}$, and $\phi = 85^\circ$, Equation (20) reduces to:

$$h_p = 0.57 \left(\frac{Q_i^2}{g \epsilon_i} \right)^{1/5} \quad (22)$$

80. If, instead of a triangular cross section, Hebbert et al. had assumed a rectangular cross section of unit width, then the difference between the plunge point depth and downstream normal depth of flow is smaller (i.e., $\zeta = \frac{h_n}{h_p} = 0.99$).

Jain

81. Jain (1981) critically examined the analysis of Savage and Brimberg (1975). He showed that the simple energy conserving model was physically unrealistic since energy dissipation near the plunge point was required for the flow mechanism, a demonstration which also invalidates the assumption that the plunge point is a stagnation point.

82. Jain also examined the gradually varied two-layer flow analysis of Savage and Brimberg (1975) by starting with the equations of Schijf and Schönfeld (1953) and assuming the mean velocity in the upper layer is zero. He concluded that the interfacial profile calculation was sensitive to the direction of numerical integration. The equations should be integrated in the direction in which the hydraulic control is acting. For mild slopes, which are characteristic of most reservoir systems, the hydraulic control is downstream and the integration should, therefore, start downstream, not at the plunge point.

83. Based on the gradually varied two-layer flow analysis, Jain proposed a nondimensional formula for the plunge point depth

$$N_p = 1.6\lambda^{0.126} N_c^{0.024} \quad (23)$$

where

$$N_p = h_p / h_n$$

$$h_n = \left(\frac{q_i^2}{g \epsilon_i} \right)^{1/3} \left(\frac{f_i + f_b}{8 S} \right)^{1/3} = \text{normal depth}$$

$$\lambda = \alpha / (1 + \alpha)$$

$$N_c = h_c / h_n$$

$$h_c = \left(\frac{q_1^2}{g \epsilon_1} \right)^{1/3} = \text{critical depth}$$

Equation (23) can be rearranged to solve for the plunge depth directly

$$h_p = 0.814 \left(\frac{\alpha}{1 + \alpha} \right)^{0.126} \left(\frac{f_1 + f_b}{S} \right)^{0.325} \left(\frac{q_1^2}{g \epsilon_1} \right)^{1/3} \quad (24)$$

Akiyama and Stefan

84. Akiyama and Stefan (1981) proposed a conceptual flow model for the plunge point which depends on inflow conditions (densimetric Froude number), downstream conditions (channel slope, roughness, and width), and mixing. Starting with the integrated momentum equation and assuming steady flow, they determined the plunge depth for a mild slope:

$$h_p = \frac{1}{2} \underbrace{\left[1 + \frac{S}{K} + \sqrt{\left(1 + \frac{S}{K} \right)^2 - \frac{4}{(1 + \gamma)^2} \frac{S}{K}} \right]}_1 \underbrace{\left(\frac{K}{S} \right)^{1/3} \left(\frac{q_1^2}{g \epsilon_1} \right)^{1/3}}_2 \underbrace{(1 + \gamma)}_3 \quad (25)$$

where

$$K = f_t / S_2 = \text{constant}$$

$$f_t = f_b + f_1 = \text{total friction factor}$$

$$S_2 = \frac{1}{\epsilon_b h_b} \int_0^\infty g \frac{\rho_a - \rho(z)}{\rho_a} dz = \text{density deficiency}$$

$$\epsilon_b = (\rho_b - \rho_a) / \rho_a = \Delta \rho_b / \rho_a$$

$$\rho_b = \text{underflow density}$$

$$h_b = \text{depth of underflow downstream of plunge point}$$

$$\gamma = \text{initial mixing coefficient}$$

$$\rho(z) = \text{density variation with depth, } z$$

and for a steep slope

$$h_p = \frac{1}{2} \left(1 + S_1 + \sqrt{(1 + S_1)^2 - \frac{4}{(1 + \gamma)^2} S} \right) \left(\frac{1}{S_1} \right)^{1/3} \left(\frac{q_i^2}{g \epsilon_i} \right)^{1/3} (1 + \gamma) \quad (26)$$

where

$$S_1 = \frac{1}{\epsilon_b h_b^2} \int_0^\infty 2g \left(\frac{\rho_a - \rho(z)}{\rho_a} \right) z \, dz = \text{density deficiency}$$

Since most reservoirs are characterized by a mild slope (i.e., $S \sim 10^{-3}$), only the solution for mild slope will be discussed hereafter.

85. The equation for plunging depth (Equation 25) on a mild slope consists of three parts. The first term on the right side of Equation (25) corresponds to depth ratio (h_p/h_b) . For mild slopes, the ratio (S/K) is small compared to 1, and Equation (25) reduces to

$$h_p = (1 + \gamma) \left(\frac{K}{S} \right)^{1/3} \left(\frac{q_i^2}{g \epsilon_i} \right)^{1/3} \quad (27)$$

Equation (27) indicates that when mixing is zero ($\gamma = 0$), the plunge depth is the normal depth downstream of the plunge point. Mixing (i.e., γ) causes the plunge depth to be larger than the normal depth. Equation (27) can be further reduced to

$$h_p = 1.1 (1 + \gamma) \left(\frac{f_t}{S} \right)^{1/3} \left(\frac{q_i^2}{g \epsilon_i} \right)^{1/3} \quad (28)$$

if it is assumed that $S_2 = 0.75$ (Ellison and Turner 1959) since

$$K = f_t/S_2.$$

Discussion

86. All of the models locate the plunge point by calculating the hydraulic depth at which the inflow plunges, which can be put in the general form:

$$h_p = \left(\frac{1}{F_p^2} \right)^{1/3} \left(\frac{Q_i^2}{W_c^2 g \epsilon_i} \right)^{1/3} \quad (29)$$

where

h_p = hydraulic depth at the plunge point

Q_i = original inflow rate

W_c = width of the zone of conveyance (the zone where the density current flows)

g = acceleration due to gravity

ϵ_i = relative density difference between the lake and inflow waters

F_p = critical densimetric Froude number

Akiyama and Stefan (1981) included a mixing term. The formulation of Hebbert et al. (1979) differs slightly from Equation (29) because they assumed a triangular instead of a rectangular cross section.

87. Before discussing the use of Equation (29), two important points need to be emphasized. First, Equation (29) solves for the hydraulic depth at the plunge point (i.e., h_p = cross-sectional area ÷ reservoir width), not the average or maximum depth. The hydraulic depth is not readily available from bathymetric maps; it must be calculated from reservoir cross-section data. The triangular cross section used in the Hebbert et al. (1979) formulation provides a unique relationship between the reservoir width, hydraulic depth, and distance along the longitudinal axis. Use of this method therefore has distinct advantages over the rectangular shaped cross section. Second, Equation (29) was developed for constant-width channels with the flow rate expressed as discharge per unit width (i.e., $q_i = Q_i/W$). Since the width is not constant for most reservoirs, Equation (29) cannot be solved directly for h_p . In addition, the width W is not the total width but the width of conveyance zone. As stated earlier, DeGray Lake is not characterized by complete lateral mixing. Even in more uniformly shaped reservoirs, density flows tend to follow the old river channel

(Kennedy et al. 1981).

88. Values of F_p typically vary from approximately 0.1 to 0.7 for a mild slope. Savage and Brimberg (1975) found $F_p = 0.5$ based on a simple energy balance. Wunderlich and Elder (1973) also found that this value correctly predicted plunge depths in Fontana Reservoir, yet there is no reason to believe that $F_p = 0.5$ should be a universal constant. Using a momentum balance, Savage and Brimberg (1975) and Akiyama and Stefan (1981) formulated F_p in terms of bed slope, bed roughness, and interfacial roughness. Once F_p is determined, the plunge depth can be calculated from Equation (29) in an iterative fashion by assuming a width and calculating a depth. The widths are continually updated until they correspond with an actual width occurring in the reservoir at the calculated hydraulic depth for the plunge point. The major problem in using Equation (29) is that the width is not always uniquely related to the hydraulic depth, especially if plug flow does not occur.

89. Using the data from the storm events and dye studies summarized in Table 1, plunge point depths were calculated with the equations recommended by Singh and Shah (1971), Wunderlich and Elder (1973), Savage and Brimberg (1975), Hebbert et al. (1979), Jain (1981), and Akiyama and Stefan (1981) (i.e., Equations 12, 15, 18, 22, 24, and 28, respectively). Site-specific parameters were:

	<u>DeGray Lake</u>	<u>West Point Reservoir</u>
S	1.2×10^{-3}	8.0×10^{-4}
f_i	0.004	0.004
f_b	0.02	0.02
f_t	0.024	0.024
α	0.2	0.2
γ	0	0
ϕ	85°	87°

Excluding the results from Singh and Shah and Akiyama and Stefan, the plunge point predictions (Table 2) were generally within ± 1 m or 20

Table 1

Summary of Inflow Studies

Date	Lake	Tracer	Flow Type	Density Current Type	Maximum Flow, m ³ /sec	Density Difference, $\epsilon_1 \times 10^4$
31 Aug 76	DeGray	Turbidity	Storm	Interflow	6.9	7.6
24 Oct 76	DeGray	Turbidity	Storm	Underflow	200	8.5
3 Mar 77	DeGray	Turbidity	Storm	Overflow	530	1.5
17 Jun 77	DeGray	Turbidity	Storm	Interflow	370	20
14 Nov 78	DeGray	Turbidity Sp. Cond.*	Storm	Interflow	500	3.5
25 Mar 79	DeGray	Dye	Base	Overflow	15	0.95
29 Mar 79	DeGray	NTU Sp. Cond. Calcium	Storm	Overflow	700	1.6
1 May 79	DeGray	Turbidity Sp. Cond.	Storm	Interflow	190	3.9
16 Jul 79	DeGray	Dye	Base	Interflow	4.6	5.6
6 Sep 79	West Point	Turbidity	Base	Underflow	89	5.2
11 Oct 79	DeGray	Dye	Base	Underflow	1.4	5.4
16 May 80	DeGray	Turbidity Sp. Cond. Calcium	Storm	Interflow	103	10.6
16 Oct 80	DeGray	Turbidity Sp. Cond. Calcium	Storm	Interflow	168	8.4
23 Jul 81	West Point	Dye	Base	Interflow	52	7.2

* Specific conductance.

Table 2
Plunge Point Depth Predictions

Date	Observed Depth,m	Width,m	Singh & Shah,m	Wunderlich & Elder,m	Savage & Brimberg,m	Hebbert et al.,m	Jain,m	Akiyama & Stefan,m
31 Aug 76	1.5	75	1.4	1.7	1.8	1.6	1.8	3.1
24 Oct 76	6.1	320	4.6	5.7	6.1	6.1	6.1	10.6
17 Jun 77	5.4	440	4.2	5.2	5.6	6.6	5.6	9.7
14 Nov 78	7.0	900	5.7	7.0	7.6	10.6	7.6	13.2
1 May 79	7.1	440	4.7	5.7	6.2	7.1	6.2	10.7
16 Jul 79	1.8	70	1.2	1.5	1.6	1.5	1.6	2.8
6 Sep 79	5.2	305	3.3	4.0	4.9	2.5	5.0	8.6
11 Oct 79	1.7	75	0.5	0.6	0.7	0.9	0.7	1.2
16 May 80	3.2	360	2.6	3.1	3.4	4.5	3.4	5.9
16 Oct 80	6.7	400	3.6	4.4	4.7	5.1	4.7	8.2
23 Jul 81	3.4	366	1.8	2.2	2.8	1.9	2.8	4.8

percent, provided the width of the zone of conveyance was used. The predictions listed in Table 2 for Hebbert et al. are one-half the result derived from Equation (22), since Equation (22) predicts the maximum plunge depth not the hydraulic depth (i.e., for a triangular cross section, the hydraulic depth is one-half the maximum depth). The predictions from the Singh and Shah equation tended to be too small while the predictions from the Akiyama and Stefan equation tended to be too large. If the total friction coefficient f_t was reduced to 0.006, then the Akiyama and Stefan predictions were almost identical to the predictions from the Savage and Brimberg equation. This finding is not unexpected since the reduced forms of Equations (18) and (28) are similar.

90. In general, the plunge point depth predictions were better for the steady base flow conditions than for the unsteady storm events. Plunge depths for storm events can be computed, however, provided the maximum flow and inflow density at the time of maximum flow were used. Attempts to use other conditions such as mean daily values or averaged , storm values were unsuccessful.

91. Sensitivity analysis on the six predictive equations indicated the results were more sensitive to perturbations in flow rate Q and conveyance width W_c than to perturbations in density differences ϵ_i . In some storm events, a change of one order in magnitude of ϵ_i resulted in a change of hydraulic depth prediction of less than 1 m, while a 50 percent change in flow (i.e., one-half the maximum flow) resulted in a change of 2 m or more. This sensitivity results from Q_i and W_c being squared in Equation (29).

92. It is recommended that the equations of Savage and Brimberg (Equation 18), Hebbert et al. (Equation 22), Jain (Equation 24), and Akiyama and Stefan (Equation 28) be used for plunge point predictions since they consider slope and friction as well as flow and density differences. They can therefore be calibrated to specific systems. It is also recommended that all four equations be used and the predictions

compared when a new or different reservoir is being evaluated. It is possible that for any specific reservoir a different equation may be more appropriate. For reservoirs that gradually expand, the Hebbert et al. equation is recommended since there is a unique relationship between width and longitudinal distance and the predicted plunge depths correspond to the maximum reservoir depths. In the other three equations, the hydraulic plunge depth is predicted and the relationship between hydraulic depth and width must be known. It must be noted, however, that the hydraulic depth may not be uniquely related to longitudinal distance.

Initial Mixing and Entrainment

93. Initial mixing and entrainment are two types of mixing phenomena important when analyzing density currents. Initial mixing includes the cumulative effects of all mixing processes acting in the vicinity of the plunge point. Entrainment occurs at the interface between the underflow and reservoir water after the inflow has plunged. Turbulence generated by bottom roughness entrains reservoir water into the underflow.

MIXING &
ENTRAINMENT
DEFINED
←

Initial Mixing

94. At the plunge point, the flow changes from a homogeneous open-channel flow to a stratified underflow. Water tends to pool at the plunge point, since it flows into the plunge zone faster than it flows out creating a large eddy (Knapp 1942, Elder and Wunderlich 1972, Ford et al. 1980). Changes in flow depth and direction all contribute to mixing. Since the mechanism is complex, the initial mixing is usually incorporated into an empirical coefficient γ defined by

$$Q_{bo} = (1 + \gamma)Q_i \quad (30)$$

where

Q_{bo} = revised flow rate including entrainment downstream of the plunge point

The density of the inflow is decreased by

$$\rho_{bo} = \frac{\gamma \rho_a + \rho_i}{(1 + \gamma)} \quad (31)$$

where

ρ_{bo} = revised inflow density after entrainment at the plunge point

95. Field data have been collected by Chasse and Slotta (1972), Elder and Wunderlich (1972), and Ford et al. (1980). Since these data may also include the effects of entrainment into the underflow (to be discussed in the next section), the mixing coefficient will be called the entrance mixing ratio r . The mixing ratio r is defined by Equations (30) and (31) with $\gamma=r$, but Q_{bo} and ρ_{bo} are defined far downstream of the plunge point. In some instances, they are the flow rate and density at the point where the underflow leaves the old river channel to become an interflow.

96. Since γ (or r) is expected to be a function of the densimetric Froude number, mixing ratios from Chasse and Slotta (1972), Elder and Wunderlich (1972), and Ford et al. (1980) are plotted versus densimetric Froude number in Figure 22. Three observations are worth noting:

- a. The data are widely scattered, with F varying from 0.1 to 0.7 and r varying from 0 to 0.8. This scatter is not unexpected considering the difficulties encountered when collecting field data of this nature and the data manipulations required to obtain F and r .
- b. Mixing ratios for specific reservoirs are more consistent and appear to be independent of F . For example, the average mixing ratios for DeGray Lake, Arkansas, Chilhowee Reservoir, Tennessee, Norris Reservoir, Tennessee, and Hills Creek Reservoir, Oregon, are 0.12, 0.03, 0.38, and 0.54, respectively.
- c. The average mixing ratio for all data is 0.26 which is consistent with the initial mixing coefficient of 0.3 recommended

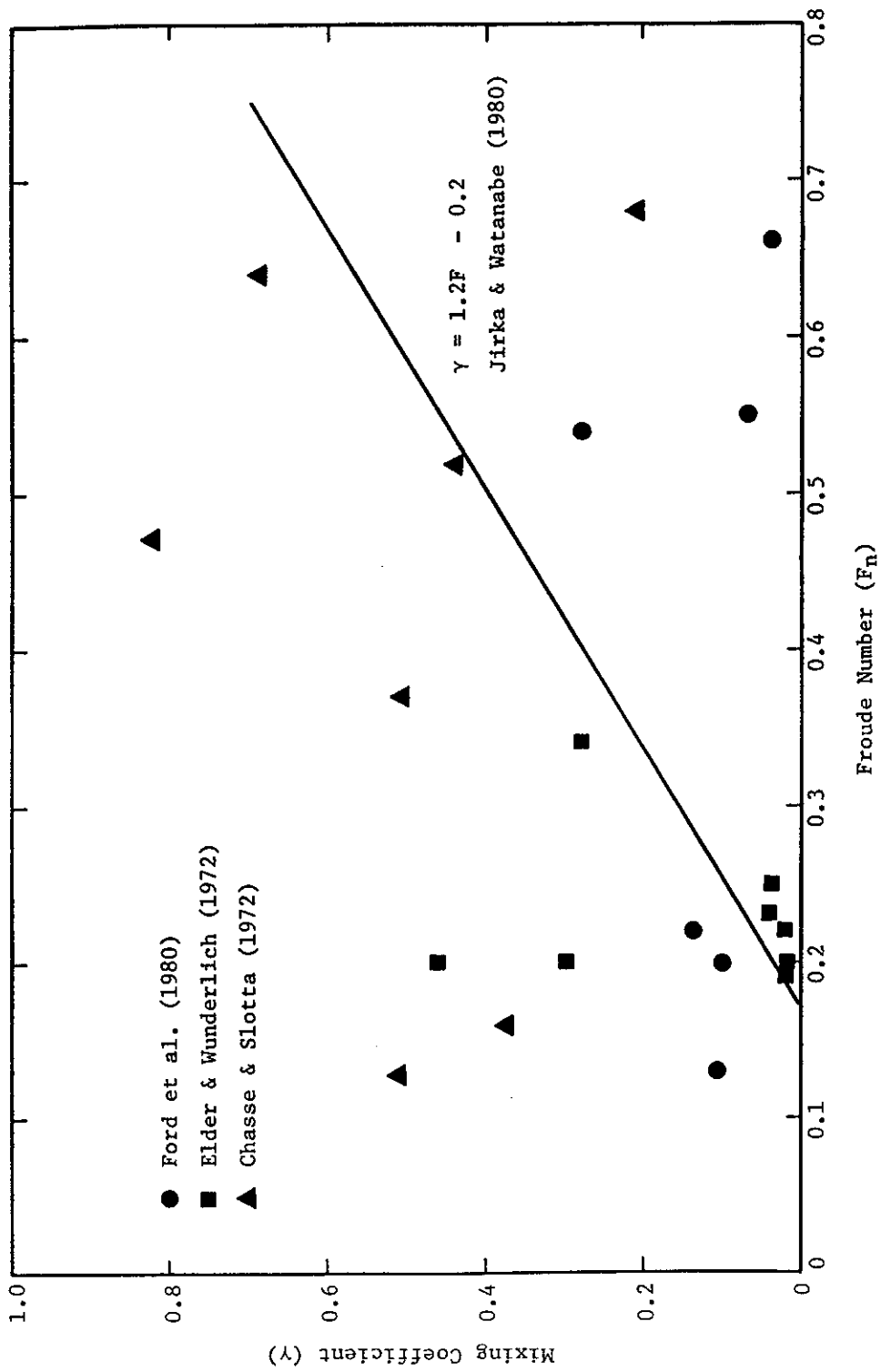


Figure 22. Relationship between the initial mixing coefficient and inflow densimetric Froude number.

by Akiyama and Stefan (1981).

97. Ryan and Harleman (1971) reported mixing ratios obtained from laboratory experiments to vary from 0.5 to 2.0. Modification of the entrance to the laboratory flume reduced the mixing ratios to between 0.1 to 0.5 indicating that the geometry of the inflowing river may be an important factor.

98. It is apparent that little is known about inflow mixing. The field data indicate that a constant entrance mixing ratio may be appropriate for specific reservoirs, but physical reasoning would indicate that the mixing ratio should be dependent on flow and the densimetric Froude number. The mixing ratio should increase as the advective forces dominate over the buoyant forces. A relationship between γ and F such that γ increases as F increases is the empirical equation.

$$\gamma = 1.2 F - 0.2 \quad (32)$$

recommended by Jirka and Watanabe (1980) for cooling ponds which is valid for $F \geq 0.167$.

Entrainment

99. After the inflow plunges, it generally follows the old river channel (thalweg) as an underflow. Turbulence generated by bottom roughness entrains reservoir water into the underflow. This second type of mixing has been analyzed by Ellison and Turner (1959), Hebbert et al. (1979), and Akiyama and Stefan (1981). Entrainment rates for an underflow can be calculated from field data using conservation of volume:

$$\frac{\partial A}{\partial t} + \frac{\partial}{\partial x}(u_b A) = E u_b B \quad (33)$$

where

u_b = mean velocity of the underflow

B = top width of the underflow

A = cross-sectional area of flow

E = the entrainment coefficient

Equation (33) assumes that the entrainment coefficient is proportional to the underflow velocity. Elder and Wunderlich (1972) and Hebbert et al. (1979) calculated entrainment rates on the order of 10^{-4} . Entrainment rates for DeGray Lake were determined to be on the order of 10^{-3} . The larger rate found in DeGray Lake may be attributed to wind-induced mixing at the bottom of the epilimnion, or to increased roughness caused by trees that were not cleared from the reservoir prior to filling (Ford and Johnson 1981).

100. The entrainment coefficient is normally assumed to be a function of the Richardson number (or densimetric Froude number). Using experimental data from Ellison and Turner (1959), Lofquist (1960), Kato and Phillips (1969), and their own experiments, Ashida and Egashira (1977) found

$$E = 0.0015 \text{ Ri}^{-1} \quad (34)$$

where

$$\text{Ri} = \frac{\Delta \rho_b}{\rho_a} \frac{g h_b}{u_b^2} = \frac{1}{F_b^2}$$

where

$\Delta \rho_b$ = density difference of underflow and ambient

h_b = depth (thickness) of underflow

Imberger and Patterson (1981) suggested

$$E = \frac{\eta^3 C_K C_b^{3/2} F_b^2}{2} \quad (35)$$

where

$\eta^3 C_K$ = mixing efficiency

C_b = bottom drag coefficient

with the efficiency $\eta^3 C_K = 3.2$ based on the field studies of Hebbert et al. (1979) and Elder and Wunderlich (1972). This mixing efficiency is a factor of 10 larger than the mixing efficiency at the bottom of the mixed layer (Imberger and Patterson 1981). Equation (35) has the

advantage of including the bottom drag coefficient, Assuming $C_b = 0.015$ (Imberger and Patterson 1981), Equation (35) becomes

$$E = 2.9 \times 10^{-3} F_b^2 = 2.9 \times 10^{-3} Ri^{-1}$$

which is similar to Equation (34).

Underflows

101. After the inflowing river passes through the plunge point zone, it moves down the submerged river channel as an underflow. The depth (thickness) of the underflow is determined by the discharge, the density of flow, and the bed and interfacial friction. Gradually varying flow theory can be used to describe the flow. If the bottom slope is mild ($S < \frac{1}{150}$ for $f_t = 0.02$), the underflow will remain subcritical and uniform flow will be achieved. If the bottom slope is steep, the flow will become supercritical downstream of the plunge point. Since most reservoir bottom slopes are mild, only mild slopes will be discussed herein. The steep slope or supercritical condition is discussed in Akiyama and Stefan (1981).

102. Following Ellison and Turner (1959), the integral method for analyzing the two-dimensional underflow is used here to avoid making assumptions concerning the shape of the velocity and density profiles. If hydrostatic equilibrium and uniform flow are assumed and if the coordinate system is taken parallel to the bottom slope such that the velocity normal to the boundary is assumed small, then, for an elemental volume of unit width, conservation of momentum is

$$\frac{d}{dx} (u_b^2 h_b) = -f_t u_b^2 - \frac{1}{2} \frac{d}{dx} (S_1 g' h_b^2 \cos \theta) + S_2 g' h_b \sin \theta \quad (36)$$

conservation of volume is

$$\frac{d}{dx} (u_b h_b) = E u_b \quad (37)$$

and conservation of mass is

$$\frac{d}{dx} (\Delta \rho_b h_b u_b) = 0 \quad (38)$$

where

h_b = depth (thickness) of underflow

f_t = total drag coefficient

E = entrainment coefficient

θ = bed slope

g' = relative acceleration of gravity = $\frac{\rho_b - \rho_a}{\rho_a} g$

$\Delta \rho_b = \rho_b - \rho_a$

S_1, S_2 = profile constants

In Equation (36), the first term on the right side is the frictional drag, the second term is the difference of the integrated hydrostatic pressure, and the last term is the gravitational force accelerating the layer. Following Akiyama and Stefan (1981), Equations (36), (37) and (38) can be manipulated to obtain

$$\frac{dh_b}{dx} = ((2 - \frac{1}{2}S_1 Ri)E - S_2 Ri \tan \theta + f_t)(1 - S_1 Ri)^{-1} Ri^{-1} \quad (39)$$

$$\frac{h_b}{3 Ri} \frac{dRi}{dx} = ((1 + \frac{1}{2}S_1 Ri)E - S_2 Ri \tan \theta + f_t)(1 - S_1 Ri)^{-1} Ri^{-1} \quad (40)$$

where

$$Ri = \frac{g' h_b \cos \theta}{u_b^2} \quad (41)$$

and it is assumed that S_1 , S_2 , and θ are independent of distance. Equations (39) and (40) can be further simplified to

$$\frac{dh_b}{dx} = E + \frac{h_b}{3Ri} \frac{dRi}{dx} = \frac{1}{Ri} \frac{\beta}{Ri^{n-1}} + \frac{h_b}{3} \frac{dRi}{dx} \quad (42)$$

if $E = \beta Ri^{-n}$.

For $n = 1$ (Ashida and Egashira 1977),

$$\frac{dh_b}{dx} = \frac{1}{Ri} \beta + \frac{h_b}{3} \frac{dRi}{dx} \quad (43)$$

For mild slopes, uniform flow is achieved downstream, Ri becomes for the normal depth R_n ; and $dRi/dx = 0$. For these conditions, Akiyama and Stefan (1981) found

$$R_n = \frac{\frac{1}{2}S_1\beta + f_t + \left[\left(\frac{1}{2}S_1\beta + f_t \right)^2 + 4\beta S_2 \tan \theta \right]^{1/2}}{2S_2 \tan \theta} \quad (44)$$

Since R_n is independent of x , Equation (43) can be integrated with respect to x to obtain:

$$h_b = \frac{\beta}{R_n} (x - x_o) + h_{bo} = E(x - x_o) + h_{bo} \quad (45)$$

where

x_o = reference point for beginning of underflow
 h_{bo} = initial depth of underflow (In practice, the initial thickness of the underflow, h_{bo} , can be estimated from the plunge depth, h_p , see Appendix C.)

From Equation (45), h_b increases linearly downstream. Equation (44) shows that as the slope increases (i.e., R_n decreases) and/or entrainment E increases, the depth of the underflow increases downstream. If there is no entrainment (i.e., if $\beta=0$), then the depth of the underflow remains constant at h_{bo} . The underflow velocity and density at point x can be determined from Equations (37), (38) and (45).

103. Hebbert et al. (1979) (see also Fischer et al. 1979 or Imberger and Patterson 1981) derived a similar relationship for a triangular cross section (Figure 21). They found

$$h_b = \frac{6}{5} E(x - x_o) + h_{bo} \quad (46)$$

where E is given by Equation (35) and

$$F_b^2 = \frac{5 \tan \theta - \frac{8}{3} E}{4E + 5C_b / \sin \phi} = \frac{2\rho_a u_b^2}{\Delta\rho_b g h_b} \quad (47)$$

Equations (35) and (47) must be solved iteratively, when C_b , θ , and ϕ are known and $\eta^3 C_K = 3.2$ is assumed. The dilution $\Delta Q/Q_i$ can then be calculated from

$$\frac{\Delta Q}{Q_i} = \left(\frac{h_b}{h_i} \right)^{5/3} - 1 \quad (48)$$

where $Q_i = u_i h_i^2 \tan \phi$ for triangular cross sections. From conservation of mass

$$(\rho_a - \rho_i)Q_i = \text{constant} \quad (49)$$

and the density of the underflow ρ_b is therefore

$$\rho_a - \rho_b = \frac{(\rho_a - \rho_i)Q_i}{Q_i + \Delta Q} \quad (50)$$

104. In summary, if the bed slope is mild (e.g., $S < 1/150$), the thickness of the underflow will be the normal depth of flow. Equations (45), (37), and (38) can be used to predict the thickness

and propagation speed of an underflow in a rectangular channel. If a triangular cross section is more representative, Equations (48) and (47) should be used. The friction factor can be obtained from a Moody diagram.

Interflows and Intrusions

105. A density interflow or intrusion occurs when a density current leaves the river bottom and propagates horizontally into a quiescent stratified fluid. The density current enters the stratified fluid at the level where the densities of the two fluids are equal. This fact distinguishes intrusions from overflows and underflows in which the densities of current and ambient fluid are not the same. Once the intrusion enters the stratified water column, all turbulence (e.g., bottom generated) quickly collapses (i.e., dissipates) and the intrusion assumes the properties of the water column. The density of the underflow at the depth where the density current enters the water column and becomes an intrusion may not be the same as the density of the river water entering the reservoir, because of the initial mixing and entrainment. Changes in flow rate and density of the current due to initial mixing and entrainment must therefore be known before an intrusion can be analyzed.

Dens of interflow
may not be same as
inflow because of
mixing
L →

106. Imberger et al. (1976) assumed that, since the intrusion is neutrally buoyant, exact symmetry exists between the inflow and outflow problem, provided the inflow momentum is small. Using the dimensionless parameter R which is defined as:

$$R = F_m Gr^{1/3} \quad (51)$$

where

$$F_m = \text{internal Froude number} = q_m / N_m L^2$$

$$Gr = \text{Grashof number} = N_m^2 L^4 / \kappa_v^2$$

$$q_m = \text{inflow per unit width at intrusion takeoff point after entrainment}$$

$$N_m = \sqrt{\frac{g}{\rho_m} \frac{d\rho}{dz}} = \sqrt{\frac{g}{\rho_m} \frac{\Delta\rho_m}{h_m}} = \text{buoyancy frequency averaged over intrusion thickness } h_m$$

$\Delta\rho_m$ = change in density over h_m

ρ_m = density at centerline of intrusion

κ_v = average vertical eddy viscosity

and the Prandtl number

$$Pr = \kappa_v / \kappa_T$$

where κ_T = average vertical diffusivity of heat. Imberger et al. (1976) defined three flow regimes:

- a. $R > 1$. The intrusion is governed by a balance between inertial and buoyancy forces. The intrusion length L_m is proportional to time t such that

$$L_m = 0.44 (q_m N_m)^{1/2} t \quad (52)$$

The intrusion speed L_m/t and thickness h_m are therefore

$$u_m = L_m/t = 0.44 (q_m N_m)^{1/2} = 0.194 \left(\frac{\Delta\rho_m g h_m}{\rho_m} \right)^{1/2} \quad (53)$$

and substituting in $u_m = Q_m / wh_m$ (assuming uniform flow) and solving for h_m yields

$$h_m = 2.99 \left(\frac{q_m^2}{\Delta\rho_m g} \right)^{1/3} \quad (54)$$

- b. $Pr^{-5/6} < R < 1$. The flow regime is dominated by a viscous-buoyancy balance. The intrusion length is

$$L_m = 0.57 LR^{2/3} t^{5/6} \quad (55)$$

and the intrusion thickness is

$$h_m = 5.5L_m Gr^{-1/6} \quad (56)$$

In this regime, 64 percent of the layer lies above the centerline (Imberger 1980). Therefore, the thickness of the intrusion above the centerline is

$$h_{m/2u} = 3.5L_m Gr^{-1/6} \quad (57)$$

and below the centerline is

$$h_{m/2l} = 2.0L_m Gr^{-1/6} \quad (58)$$

c. $R < P_r^{-5/6}$. This flow regime is dominated by viscosity and diffusion. The intrusion length is

$$L_m = CLR^{3/4} Gr^{-1/8} \quad (59)$$

and the thickness is of the order $LGr^{-1/6}R^{1/5}$. The coefficient C is unknown.

107. The coefficients in Equations (52) and (55) were obtained using laboratory data from Zuluaga-Angel et al. (1972), Maxworthy (1972), and Manins (1976) and verified with data from Silvester (1979). The predictive equations were also compared with field data from Cherokee, Fontana, and Wellington Reservoirs. Cherokee and Fontana Reservoirs were in the inertial regime ($R > 1$), while Wellington was in the viscous regime. According to Imberger (1980), Equations (54), (57) and (58) underpredict the thickness of the flow zone.

108. Manins (1976) obtained similar results for the inertial range and went on to show that internal waves (shear waves) affect the intrusion thickness and to a lesser extent the intrusion

speed. The effect of the internal waves is to adjust the isopycnals (lines of constant density) so that they return to a horizontal position at steady state (Mahony and Pritchard 1977).

109. Unless dissolved solids dominate the density profile (i.e., high Pr), intrusions in most reservoirs fall into the inertial range and Equations (52), (53), and (54) should be used. These equations were therefore used to analyze the interflows summarized in Table 1. The intrusion centerline was assumed to be the depth in the lake where the lake temperature (i.e., density) and inflow temperature (density), including the effects of inflow mixing, matched. The total inflow per unit width was obtained by dividing the total inflow (including inflow mixing) by the average reservoir width of the zone of conveyance at the intrusion centerline level. The upper and lower half-thicknesses of the intrusion were then computed separately using Equation (54) and assuming the total inflow per unit width was equally divided above and below the centerline (i.e., q_m was divided by 2 in Equation 54 and the resulting h_m was the half-thickness). This procedure was followed to account for temperature (density) profiles that were not symmetrical about the intrusion centerline. The actual application of Equation (54) involved assuming a half-thickness h_{m2}^1 , calculating the $\Delta\rho_m$ over h_{m2}^1 from the temperature (density) profile, and finally calculating h_{m2}^1 . This process was continued until the assumed h_{m2}^1 converged on the computed h_{m2}^1 , which normally occurred within 3 iterations with judicious choices of h_{m2}^1 .

110. Initial computations using the maximum flow rate, as recommended for the plunge point calculation, resulted in intrusion thicknesses that were too large. Subsequent analyses indicated that correct intrusion thicknesses could be computed if the flow rates were averaged over the time scale required for the intrusion to pass through the lake. This time scale was computed from Equation (53) with L_m equal to the length of the lake, and $\Delta\rho_m$ and h_m taken across the metalimnion. For typical summer stratification conditions in DeGray Lake, the appropriate time scale was 4 days. During the spring and fall, when the

stratification is weaker, the time scale increases to 6 or more days. When a time scale of 4 days for the summer months and 6 days for early spring and late fall was used, the following results were obtained from Equation (54):

Date	Observed		Predicted	
	h_{m2u}, m	h_{m2l}, m	h_{m2u}, m	h_{m2l}, m
31 Aug 76	1.8	2.2	1.8	2.0
17 Jun 77	3.0	2.0	2.8	2.4
14 Nov 78	3.8	2.3	3.4	2.8
1 May 79	5.5	4.0	5.8	5.5
16 Jul 79	2.4	1.1	2.4	1.4
23 Jul 81	2.0	2.0	1.9	1.9

An example of these computations is given in Appendix B.

111. The total intrusion thicknesses predicted by Equation (54) were usually within 0.5 m or 20% of the observed values, provided the correct time scale was used to average the storm flows and the width of the zone of conveyance was used to obtain the discharge per unit width. For any specific reservoir, the time scale can be computed from Equation (53) assuming L_m equals the reservoir length, $\Delta\rho_m$ equals the average density difference between the epilimnion and hypolimnion, and h_m equals the average thickness of the metalimnion. Selection of the width for the zone of conveyance requires extensive knowledge of the reservoir hydrodynamics and flow patterns. In general, side arms, and dead-end coves should not be included in the conveyance width (Figure 23). Aerial overflights after major storm events (e.g., Figure 5) may provide insight into flow patterns. For hand computations of specific events, conveyance widths should be obtained from cross-sectional data in the region of the reservoir of interest (e.g., the upper end). If the interflow enters the pool at an elevation where uncleared timber may determine the conveyance limits, sonar soundings such as those reproduced

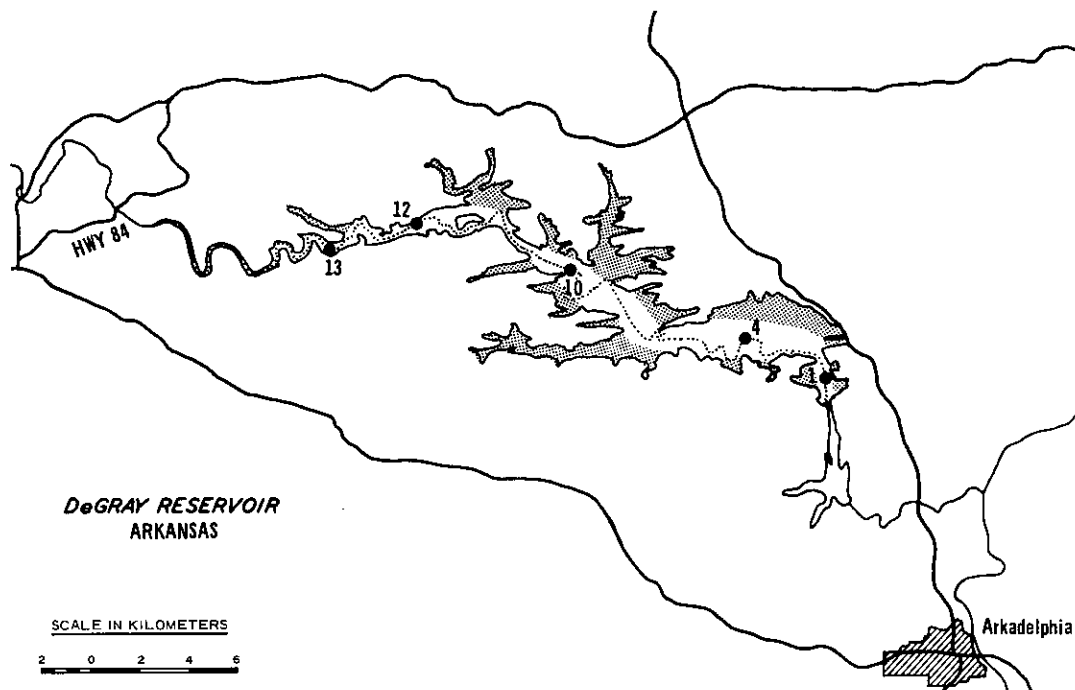


Figure 23. Zone of conveyance for DeGray Lake, AR.

in Figure 6 may also be helpful. For mathematical model simulations (e.g., CE-QUAL-R1), the conveyance width should be selected to be representative of the lower region of the reservoir near the dam.

112. Once the intrusion thicknesses are computed from Equation (54), the intrusion speed can be computed from Equation (53) using the total density difference $\Delta\rho_m$ across the total intrusion thickness h_m . The following results were obtained:

<u>Date</u>	<u>Observed Speed, m/sec</u>	<u>Predicted Speed, m/sec</u>
31 Aug 76	0.05	0.05
17 Jun 77	0.06	0.06
1 May 79	0.06	0.04
16 Jul 79	0.03	0.05
23 Jul 81	0.03	0.03

The observed speeds were for movement of the center of mass and not the leading edge, which moved at a faster rate. For the storm flows, the observed speed was averaged over 3 or 4 days and did not consider the period when the flows stalled (paragraph 39).

113. In general, the predicted intrusion speeds were of the correct order of the magnitude. It must be emphasized, however, that the accuracy of these predictions is highly dependent on the accuracy of the thickness computations. Equation (53) assumes that buoyancy forces drive the intrusion. Therefore, in reservoirs dominated by advective forces, the accuracy of the predictions may be questionable.

114. Equations (54) and (53) are recommended to compute intrusion thicknesses and speeds. They can be used for both base and storm flows provided the flows are averaged over the proper time scale and the width for the zone of conveyance is used.

PART IV: SUMMARY AND RECOMMENDATIONS

Review Summary

115. A literature review of field studies on density currents in reservoirs produced the following findings:

- a. Analysis of field data on density currents is complicated by irregular reservoir morphometry, unsteady and multiple tributary inflows, variable stratification, and man-made perturbations.
- b. Old roadways, railroad crossings, cofferdams, causeways, constrictions, and other hidden obstructions can cause irregularities in or blocking of the anticipated flow field.
- c. In many reservoirs, the flow path follows the old thalweg, with incomplete lateral mixing. The appropriate width and length scales therefore appear to be the width and length of the old river channel or zone of conveyance.
- d. Transport into and out of coves, embayments, etc., is enhanced with pool-level fluctuations. When the pool level is rising, water moves back into the embayments. During periods of falling pool levels, water moves out of the coves.
- e. When inflows enter a wide lake (i.e., width > 1 km) in the northern hemisphere, Coriolis accelerations cause the density interfaces to tilt to the right side of the basin.
- f. Inflowing water tends to pool at the plunge point, which can result in water quality problems. The pooling enhances delta formation.
- g. The location of the plunge point is highly dynamic. It can move several kilometers in a few hours in response to dynamic flow events such as a storm event or hydropower generation.
- h. For reservoirs characterized by mild slopes (e.g. 10^{-3}), initial mixing and entrainment are small, averaging about 25 percent.

- i. Interflows (intrusions) stall and collapse when there is no hydraulic gradient (i.e., inflow or outflow).
- j. Even when a stable underflow or interflow occurs, inflow materials can still be transported to the surface waters by wind-generated mixing mechanisms and changes in meteorological conditions.

Predictive Techniques

116. All of the predictive techniques analyzed in this study worked well under laboratory conditions (i.e., steady and uniform flow, uniform channels and geometry, and linear stratification); however, the application of these techniques to existing reservoirs is complicated by irregular morphometry, varying inflow characteristics, varying stratification, and reservoir operation. Many reservoirs are dendritic in shape and characterized by nonuniform widths, varying bottom roughness, islands, and multiple tributaries. Inflow characteristics, such as flow, temperature, and TDS and SS concentrations, vary diurnally, synoptically (storm events), and seasonally. In-lake density stratification is dynamic, nonlinear, and sometimes unstable. Changes in reservoir operation (i.e., rule curve, withdrawal depth, release rate, etc.) can have a significant effect on inflow density currents and are not considered in any of the predictive techniques.

117. The recommended predictive techniques are described hereafter and sample applications are presented in Appendix B.

Overflows

118. Overflows occur when the inflowing water density is less than the reservoir water surface density. This condition typically occurs in the spring when rivers warm more rapidly than reservoirs. Predictive equations are available for the separation point (Equation 1), overflow thickness (Equation 10), and frontal propagation speed (Equation 8). The separation point is analogous to the plunge point. Since overflows are exposed to wind-induced mixing mechanisms and heat transfer at the

air-water interface, predictions are susceptible to large errors and should be used with caution. Predictions of separation point depths for the overflows in Table 1 were in error by over 100 percent.

Plunge Point Location

119. Density inflows plunge beneath the water surface when the buoyancy forces balance the advective forces. The plunge point location is determined by computing the hydraulic depth at which the flow plunges. Several investigators have proposed formulas for this depth assuming steady state, uniform velocity and density profiles, and constant reservoir density, among other assumptions. The formulas typically depend on the inflow densimetric Froude number, bed slope, and friction coefficients. Akiyama and Stefan (1981) (Equation 28) included initial mixing, which increased the depth of the plunge point. Equations (18), (22), (24), and (28) predicted the plunge point depths to within ± 1 m (i.e., 1 km along the longitudinal axis) for both base flow and storm events. No specific formulation is recommended since no one formula is superior for all reservoirs. The formula of Hebbert et al. (1979) (Equation 22) is used in the computer algorithm (Appendix C), since it employs a triangular cross section and there is a unique relationship between reservoir depth, width and longitudinal distance. It is recommended, however, that the width of the zone of conveyance be used in Equations (18), (24), and (28) if known.

Underflows

120. After the inflow plunges, it moves along the submerged river channel as an underflow. Turbulence generated at the bed entrains ambient reservoir water into the underflow. If the bed slope is mild (e.g., $S < 1/150$), Equations (45), (37), and (38) can be used to predict the thickness and propagation speed of an underflow in a rectangular channel. If a triangular cross section is used, Equations (46) and (48) can be used.

Interflows (Intrusions)

121. Intrusions occur when an underflow leaves the old river

channel and propagates horizontally into a stratified water column at a level of neutral buoyancy. The intrusion problem is therefore analogous to the withdrawal problem in a stratified fluid. Equations (54) and (53) can be used to estimate the intrusion thickness and speed, respectively, for the nonviscous regime. The width for the zone of conveyance should be used to compute the discharge per unit width, and storm flows should be averaged over the appropriate time scale, which is computed from Equation (52).

REFERENCES

- Adams, E. E., Stolzenbach, K. D., and Harleman, D. R. F. 1975. Near and far field analysis of buoyant surface discharges into large bodies of water. Report No. 205. Ralph M. Parsons Laboratory for Water Resources and Hydrodynamics, Massachusetts Institute of Technology, Cambridge, Mass.
- *Akiyama, J., and Stefan, H. G. 1981. Theory of plunging flow into a reservoir. St. Anthony Falls Hydraulic Laboratory Internal Memorandum I-97. Minneapolis, Minn.
- *Ashida, K., and Egashira, S. 1977. Hydraulic characteristics of thermocline in reservoirs. Proc. 17th Cong. International Association for Hydraulic Research. 2:33-40.
- Bayne, D. B. 1967. A procedure for detection of flow-dispersion patterns on a large impoundment. Master of Science Thesis. Auburn University, Auburn, Alabama.
- Bell, H. S. 1942. Density currents as agents for transporting fine sediments. J. of Geol. L, 5:512-547.
- Benjamin, T. B. 1968. Gravity currents and related phenomena. J. Fluid Mech. 31:209-248.
- Carmack, E. C. 1979. Combined influence of inflow and lake temperature on spring circulation in a riverine lake. J. Phys. Oceanogr. 9:422-434.
- Chasse, J., and Slotta, L. S. 1972. Field studies of reservoir currents. U. S. Army Engineer Hydrologic Engineering Center, Davis, Calif. Contract Report No. DACW05-71-C-0110.
- Chen, C. T., and Millero, F. J. 1977. The use and misuse of pure water PVT properties for lake waters. Nature. 266:707-708.
- Churchill, M. A. 1958. Effects of storage impoundments on water quality. Trans. Am. Soc. Civ. Eng. 123:419-464.
- Churchill, M. A. 1965? Effects of density currents in reservoirs on water quality. Water and Sewage Works. Reference Number 1965.
- Elder, R. A., and Wunderlich, W. O. 1968. Evaluation of Fontana Reservoir field measurements. Technical Report No. 17. Department of Environmental and Water Resources Engineering, Vanderbilt University, Nashville, Tenn.

Elder, R. A., and Wunderlich, W. O. 1972. Inflow density currents in TVA reservoirs. Proc. Int. Symp. Stratified Flow. Am. Soc. Civil Eng. 221-229.

Ellison, T. H., and Turner, J. S. 1959. Turbulent entrainment in stratified flows. J. Fluid Mech. 6:423-448.

Environmental Laboratory. 1982. CE-QUAL-R1: A numerical one-dimensional model of reservoir water quality; User's manual. Instructional Report E-82-1. U. S. Army Engineer Waterways Experiment Station, CE, Vicksburg, Miss.

Fischer, H. B., List, E. J., Koh, R. Y. C, Imberger, J. and Brooks, N. H. 1979. Mixing in Inland and Coastal Waters. Academic Press. NY.

Fischer, H. B., and Smith, R. D. 1982. Observations of transport to surface waters from a plunging inflow to Lake Mead. Limnol. Oceanog. In Press.

Ford, B., and Ford, D. E. 1982. The hydrometeorology of DeGray Lake, Arkansas. Technical Report in press. U. S. Army Engineer Waterways Experiment Station, CE, Vicksburg, Miss.

Ford, D. E., and Johnson, M. C. 1981. Field observations of density currents in impoundments. Proc. Symp. Surface Water Impoundments, H. G. Stefan, ed. American Society of Civil Engineers. pp 1239-1248.

Ford, D. E., Johnson, M. C., and Monismith, S. G. 1980. Density inflows to DeGray Lake, Arkansas. Proc. 2nd International Symp. on Stratified Flows. International Association for Hydraulic Research. 2:977-987.

Fry, A. D., Churchill, M. A., and Elder, R. A. 1953. Significant effects of density currents in TVA's integrated reservoir and river system. Proc. Minnesota International Hydraulics Convention. Joint Meeting International Association for Hydraulic Research and American Society of Civil Engineers. pp 335-354.

Grover, N. C., and Howard, C. S. 1938. The passage of turbid water through Lake Mead. Trans. Am. Soc. Civ. Eng. 103:720-732.

Hamblin, P. F., and Carmack, E. C. 1978. River-induced currents in a fjord lake. J. Geophy. Res. 83:885-899.

Harleman, D. R. F. 1961. Stratified flow. Handbook of Fluid Dynamics, V. Streeter, ed. McGraw-Hill, New York.

Harleman, D. R. F. 1975. Heat disposal in the environment. J. Hydraul. Div. Proc. Am. Soc. Civ. Eng. 101(HY9):1120-1138.

Hebbert, B., Imberger, J., Loh, I., and Patterson, J. 1979. Collie River underflow into the Wellington Reservoir. J. Hydraul. Div. Proc. Am. Soc. Civ. Eng. 105(HY5):533-545.

Imberger, J. 1980. Selective withdrawal: A review. Proc. 2nd International Symp. on Stratified Flow. International Association for Hydraulic Research, T. Carstens and T. McClimans, eds. Tapir, Trondheim, Norway.

Imberger, J., and Patterson, J. C. 1981. A dynamic reservoir simulation model - DYRESM:5. Transport Models for Inland and Coastal Waters. H. Fischer, ed. Academic Press. 310-361.

Imberger, J., Thompson, R. and Fandry, C. 1976. Selective withdrawal from a finite rectangular tank. J. Fluid Mech. 78:389-412.

Jain, S. C. 1981. Plunging phenomena in reservoirs. Proc. Symp. Surface Water Impoundments, H. G. Stefan, ed. American Society of Civil Engineers. pp 1249-1257.

Jirka, G. H., and Watanabe, M. 1980. Thermal structure of cooling ponds. J. Hydraul. Div. Proc. Am. Soc. Civ. Eng. 106(HY5):701-715.

Johnson, M. C. 1983. Fluorometric techniques for tracing inflows in reservoirs. Instructional Report in Preparation. U. S. Army Engineer Waterways Experiment Station, CE, Vicksburg, Miss.

Johnson, M. C., Ford, D. E., Buchak, E. M. and Edinger, J. E. 1981. Analyzing storm event data from DeGray Lake, Arkansas, using LARM. Presented at 1981 American Society of Civil Engineers Convention and Exposition. St. Louis, Mo.

Johnson, M. C., Ford, D. E., and Waide, J. B. 1983. Observations of density currents in Lake DeGray, Arkansas. Technical Report in Preparation. U. S. Army Engineer Waterways Experiment Station, CE, Vicksburg, Miss.

Johnson, N. M., and Merritt, D. H. 1979. Convective and advective circulation of Lake Powell, Utah-Arizona, during 1972-1973. Water Resources Res. 15(4):873-884.

Kao, T. W. 1976. Principal stage of wake collapse in a stratified fluid, two-dimensional theory. Physics of Fluids. 19:1071-1074.

Kao, T. W. 1977. Density currents and their applications. J. Hydraul. Div. Proc. Am. Soc. Civ. Eng. 103(HY5):543-555.

Karman, T. von. 1940. The engineer grapples with nonlinear problems. Bull. Am. Math. Soc. 46:615-683.

Kato, H. and Phillips, O. M. 1969. On the penetration of a turbulent layer into a stratified fluid. J. Fluid Mech. 37:643-655.

Kennedy, R. H., Gunkel, R. C. and Carlile, J. M. 1983. Riverine influence on the water quality characteristics of West Point Lake. Technical Report in preparation, U. S. Army Engineer Waterways Experiment Station, CE, Vicksburg, Miss.

Kennedy, R. H., Thornton, K. W. and Carroll, J. H. 1981. Suspended sediment gradients in Lake Red Rock. Proc. Symp. Surface Water Impoundments, H. G. Stefan, ed. American Society of Civil Engineers. 1318-1328.

Kennedy, R. H., Thornton, K. W. and Gunkel, R. C. 1982. Establishment of water quality gradients in reservoirs. Can. Wat. Res. J. 7(1):71-87.

Keulegan, G. H. 1957. An experimental study of the motion of saline water from locks into fresh water-channels. Nat. Bur. Stand. Rep. 5168. Washington, D.C.

Knapp, R. T. 1942. Density currents: Their mixing characteristics and their effect on the turbulence structure of the associated flow. Proc. of the Second Hydraulic Conference. State University of Iowa, Iowa City. pp 289-306.

Koh, R. C. Y. 1976. Buoyancy-driven gravitational spreading. Proc. 15th International Coastal Engineering Conference. Honolulu, Hawaii. pp 2956-2975.

Koryak, M., Stafford, L. J., and Montgomery, W. H. 1979. The limnological response of a West Virginia multipurpose impoundment to acid inflows. Water Resources Res. 15(4):929-934.

Lofquist, K. 1960. Flow and stress near an interface between stratified liquids. Physics of Fluids. 3:158-175.

Mahony, J. J., and Pritchard, W. G. 1977. Withdrawal from a reservoir of stratified fluid. Report No. 79. Fluid Mech. Res. Inst., University of Essex, England.

Manins, P. C. 1976. Intrusion into a stratified fluid. J. Fluid Mech. 74:547-560.

Maxworthy, A. 1972. Experimental and theoretical studies of horizontal jets into stratified fluid. Proc. Int. Symp. Stratified Flow. American Society of Civil Engineers.

Middleton, G. V. 1966. Experiments on density and turbidity currents 1. Motion of the head. Can. J. Earth Sci. 3:523-546.

Morris, M. W., and Thackston, E. L. 1969. Tracing polluted reservoir inflows with fluorescent dyes. Technical Report No. 21. Environmental and Water Resources Engineering. Vanderbilt University, Nashville, Tenn.

Nix, J. 1981. Contribution of hypolimnetic water on metalimnetic dissolved oxygen minima in a reservoir. Water Resources Res. 17(2): 329-332.

Perrier, E. R., Westerdahl, H. E., and Nix, J. F. 1977. Water quality loadings during thirteen storms in the Caddo River, Arkansas. Am. Soc. Agr. Engr. Meeting, Paper No. 77-2529, St. Joseph, Mich.

Ryan, R. J. and Harleman, D. R. F. 1971. Prediction of the annual cycle of temperature changes in a stratified lake or reservoir: Mathematical model and user manual; Massachusetts Institute of Technology, Cambridge. Department of Civil Engineering. R. M. Parsons Laboratory for Water Resources and Hydrodynamics. Technical Report No. 137.

Safaie, B. 1979. Mixing of buoyant surface jet over sloping bottom. J. Waterways Port Coastal and Ocean Eng. Div., Proc. Am. Soc. Civ. Eng. 105(WW4):357-373.

Savage, S. B., and Brimberg, J. 1975. Analysis of plunging phenomena in water reservoirs. J. Hydraulic Research. 13(2):187-204.

Schijf, J. B., and Schönfeld, J. C. 1953. Theoretical considerations on the motion of salt and fresh water. Proc. Minnesota Inter. Hydr. Confr.. International Association for Hydraulic Research. 321-333.

Serruya, S. 1974. The mixing patterns of the Jordan River in Lake Kinneret. Limnol Oceanogr. 19(2):175-181.

Silvester, R. 1979. An experimental study of end wall effects on selective withdrawal of linearly stratified liquid from a reservoir. Ph.D. Thesis, University of Western Australia, Nedlands, Western Australis.

Singh, B., and Shah, C. R. 1971. Plunging phenomenon of density currents in reservoirs. LaHouille Blanche. 26(1):59-64.

Soltero, R. A., Wright, J. C., and Horpestad, A. A. 1974. The physical limnology of Bighorn Lake - Yellowtail Dam, Montana: Internal density currents. Northwest Science. 48(2):107-124.

Stigebrandt, A. 1978. Dynamics of an ice-covered lake with through-flow. Nordic Hydrology. 9:219-244.

Sutron Corporation. 1980. Study of the lateral and longitudinal mixing characteristics of the Missouri River in Lewis and Clark Lake. Sutron Report No. SCR-348-80-035 for U. S. Army Engineer Division, Missouri River, Omaha, Neb.

Thornton, K. W., Nix, J. F., and Bragg, J. D. 1980. Coliforms and water quality: Use of data in project design and operation. Water Resources Bulletin. 16(1):86-92.

Thornton, K. W., Kennedy, R. H., Carrol, J. H., Walker, W. W., Gunkel, R. C., and Ashby, S. 1981. Reservoir sedimentation and water quality - An heuristic model. Proc. Symp. Surface Water Impoundments, H. G. Stefan, ed. American Society of Civil Engineers. pp 654-661.

Turner, J. S. 1973. Buoyancy Effects in Fluids. Cambridge University Press, England.

Vanoni, V. A. 1975. Sedimentation Engineering. ASCE - Manuals and Reports on Engineering Practice. No. 54. American Society of Civil Engineers. New York.

Westerdahl, H. E., Ford, W. B. III, Harris, J., and Lee, C. R. 1981. Evaluation of techniques to estimate annual water quality loadings to reservoirs. Tech. Report E-81-1. U. S. Army Engineer Waterways Experiment Station, CE. Vicksburg, Miss.

Wiebe, A. H. 1939. Density currents in Norris Reservoir. Ecology. 20(3):446-450.

Wilkinson, D. L. 1972. Dynamics of contained oil slicks. J. Hydraul. Div. Proc. Am. Soc. Civ. Eng. 98(HY6):1013-1030.

Wilkinson, D. L. 1973. Limitations to length of contained oil slicks. J. Hydraul. Div. Proc. Am. Soc. Civ. Eng. 99(HY5):701-711.

Wilkinson, D. L., and Wood, I. R. 1972. Some observations on the motion of the head of a density current. J. Hydraul. Res. 10:305-324.

Wood, I. R. 1966. Studies in unsteady self preserving turbulent flows. Rept. No. 81. Water Research Lab, Univ. of New South Wales.

Wunderlich, W. O., and Elder, R. A. 1973. Mechanics of flow through man-made lakes. Man-Made Lakes: Their Problems and Environmental Effects, W. C. Ackermann, G. F. White and E. B. Worthington, eds. American Geophysical Union, Washington, D.C.

Zuluaga-Angel, A., Darden, R. B., and Fischer, H. B. 1972. Flow into a stratified reservoir. U. S. Environmental Protection Agency Report No. R2-72-037. Washington, D. C.

APPENDIX A: DENSITY OF WATER

1. The density of water is a function of temperature, total dissolved solids, and suspended solids:

$$\rho_w = \rho_T + \Delta\rho_{TDS} + \Delta\rho_{SS} \quad (A1)$$

where

$$\begin{aligned} \rho_w &= \text{water density, kg/m}^3 \\ \rho_T &= \text{water density resulting from temperature variations, kg/m}^3 \\ \Delta\rho_{TDS} &= \text{density increment due to total dissolved solids, kg/m}^3 \\ \Delta\rho_{SS} &= \text{density increment due to suspended solids, kg/m}^3 \end{aligned}$$

2. Many different formulations have been proposed for determining the density variation due to temperature. Several mathematical models used

$$\rho_T = 1000. - \frac{(T - 3.98)^2 (T + 283)}{(503.57) (T + 67.26)} \quad (A2)$$

where

T = water temperature, $^{\circ}\text{C}$.

Eq. (A2) attains a maximum density of $1000. \text{ kg/m}^3$ at $T = 3.98^{\circ}\text{C}$.

3. A simpler and computationally more efficient relationship is

$$\begin{aligned} \rho_T &= 999.841 + 6.59583 \times 10^{-2} T - 8.45123 \times 10^{-3} T^2 \\ &\quad + 5.29159 \times 10^{-5} T^3 \end{aligned} \quad (A3)$$

Chen and Millero (1977) proposed

$$\begin{aligned} \rho_T &= 999.8395 + 6.7914 \times 10^{-2} T - 9.0894 \times 10^{-3} T^2 \\ &\quad + 1.0171 \times 10^{-4} T^3 - 1.2846 \times 10^{-6} T^4 + 1.1592 \times 10^{-8} T^5 \end{aligned} \quad (A4)$$

$$- 5.0125 \times 10^{-11} T^6$$

4. The density increment due to total dissolved solids is

$$\Delta \rho_{\text{TDS}} = \rho_{\text{TDS}} * C_{\text{TDS}} \quad (\text{A5})$$

where

$$\rho_{\text{TDS}} = \text{density conversion factor, kg/m}^3/\text{g/m}^3$$

$$C_{\text{TDS}} = \text{TDS concentration, g/m}^3$$

Reported values for ρ_{TDS} vary from less than 0.0005 to 0.001; a typical value is 0.00078. ρ_{TDS} will depend on the chemical makeup of the TDS and temperature. Chen and Miller found

$$\rho_{\text{TDS}} = 8.221 \times 10^{-4} - 3.87 \times 10^{-6} T + 4.99 \times 10^{-8} T^2 \quad (\text{A6})$$

5. The density increment due to suspended solids is

$$\Delta \rho_{\text{SS}} = C_{\text{SS}} (1 - 1/\text{SG}) \times 10^{-3} \quad (\text{A7})$$

where

$$C_{\text{SS}} = \text{SS concentration, g/m}^3$$

SG = specific gravity of the suspended solids

For a SG = 2.65, Eq. (A7) reduces to

$$\Delta \rho_{\text{SS}} = 0.00062 C_{\text{SS}} \quad (\text{A8})$$

6. Chen and Millero also modified the density for pressure (i.e., at depth):

$$\rho_{\text{wp}} = \rho_{\text{w}} / (1 - P/K) \quad (\text{A9})$$

where

$$\begin{aligned}
 P &= \text{pressure, bars (1 bar} \approx 10.2 \text{ m of water)} \\
 K &= 19652.17 + 148.376T - 2.329T^2 \\
 &\quad + 1.3963 \times 10^{-2} T^3 - 5.90 \times 10^{-5} T^4 \\
 &\quad + (3.2918 - 1.719 \times 10^{-3} T + 1.684 \times 10^{-4} T^2) P \\
 &\quad + (-0.8985 + 2.428 \times 10^{-2} T + 1.114 \times 10^{-2} P) \times 10^{-3} \times \text{TDS}
 \end{aligned}
 \tag{A10}$$

The effect of pressure on water quality density is shown in Figure A1. For depths greater than 100 m, the pressure effect can be significant.

7. Any of the above formulations can be used for simple density computations provided formulations are not mixed. For more accurate computations, Eqs. (A1), (A4), (A6), (A9), and (A10) are recommended. These equations have a precision of $2 \times 10^{-3} \text{ kg/m}^3$ over the range 0-30°C, 0-600 ppm TDS, and 0-180 bars.

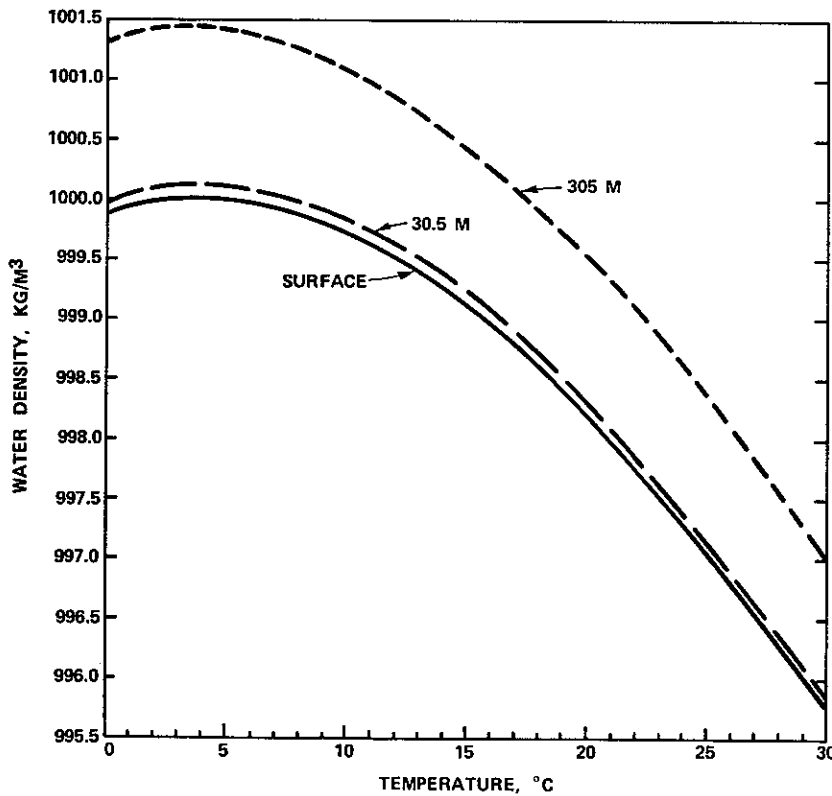


Figure A1. Effect of hydrostatic pressure (depth) on water density.

APPENDIX B: EXAMPLE COMPUTATIONS

1. In this appendix, two examples from DeGray Lake, Arkansas, are presented to illustrate the use of the recommended predictive equations for plunge point location, initial mixing, interflow thickness, and propagation speed. The first example is a dye study which was performed in July 1979 under steady flow conditions ($Q_i = 4.6 \text{ m}^3/\text{sec}$), where, after plunging, the dye moved into the reservoir as an interflow (Figure B1). The second example is an unsteady storm event which occurred in June 1977, when the flow increased from approximately $5 \text{ m}^3/\text{sec}$ to $370 \text{ m}^3/\text{sec}$ in 8 hours (Figure B2) and the turbid storm water entered the lake as an interflow. Both of these examples are fully described in Johnson et. al. (1983).

July 1979 Dye Study

2. At the time of dye injection, the following conditions were measured:

Flow rate $Q_i = 4.6 \text{ m}^3/\text{sec}$

Inflow temperature $T_i = 27.9^\circ\text{C}$

River cross-sectional area $A = 7.2 \text{ m}^2$

River top width $W = 24.7 \text{ m}$

Hydraulic depth $h_i = A/W = 0.3 \text{ m}$

Lake surface temperature $T_a = 29.5^\circ\text{C}$

Using Equation (A2) for the density of water,

$$\rho_i = 996.288 \text{ kg/m}^3$$

$$\rho_a = 995.733 \text{ kg/m}^3$$

The inflow densimetric Froude number F_i (Equation 2) is:

$$F_i = \frac{u_i}{(\epsilon_i g h_i)^{1/2}} = \frac{(4.6/7.2)}{[(5.6 \times 10^{-4}) * 9.8 * 0.3]^{1/2}} = 16$$

where

$$u_i = Q_i/A$$

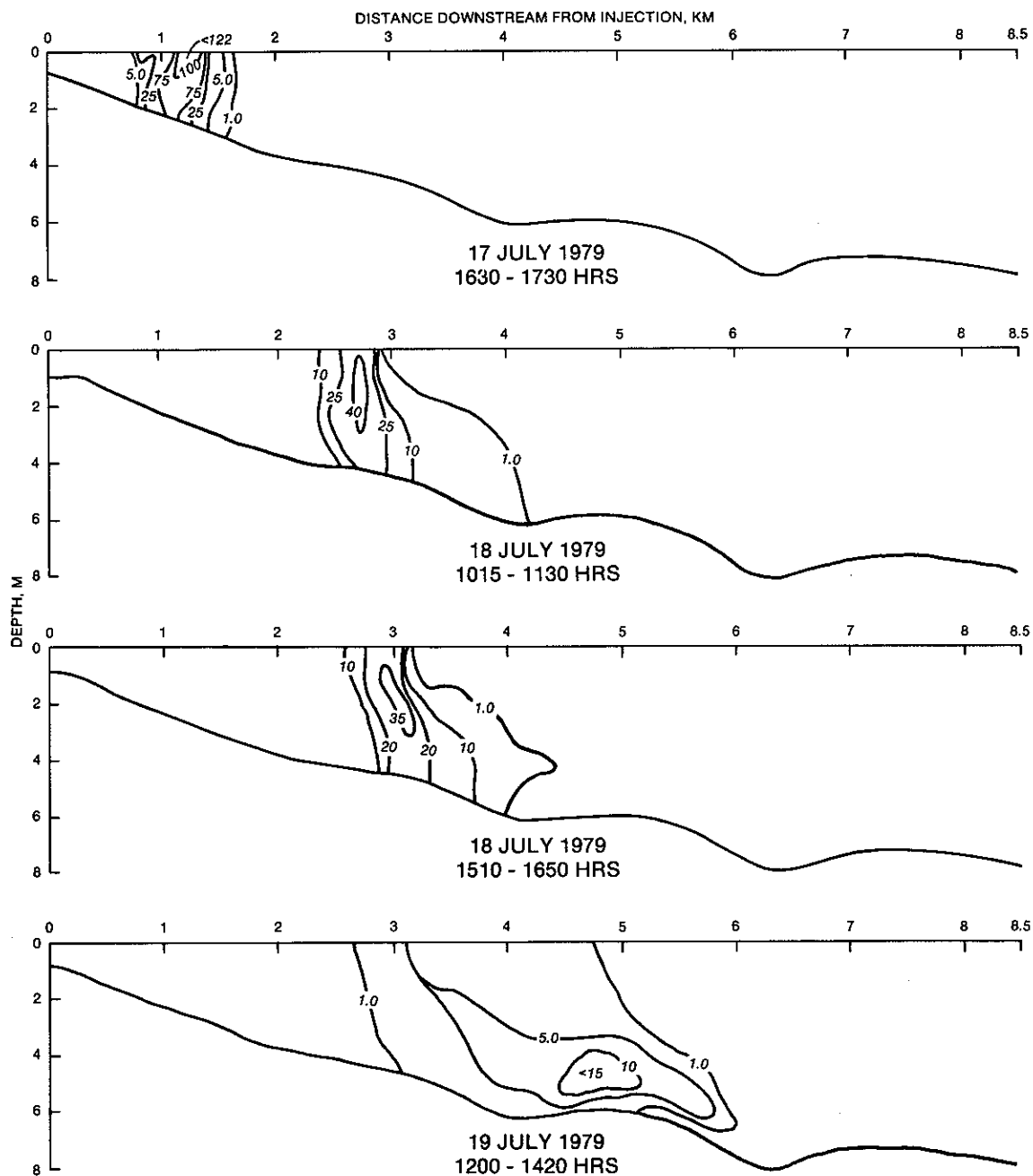


Figure B1. Dye concentrations in ppb for the July 1979 dye study, DeGray Lake, Arkansas.

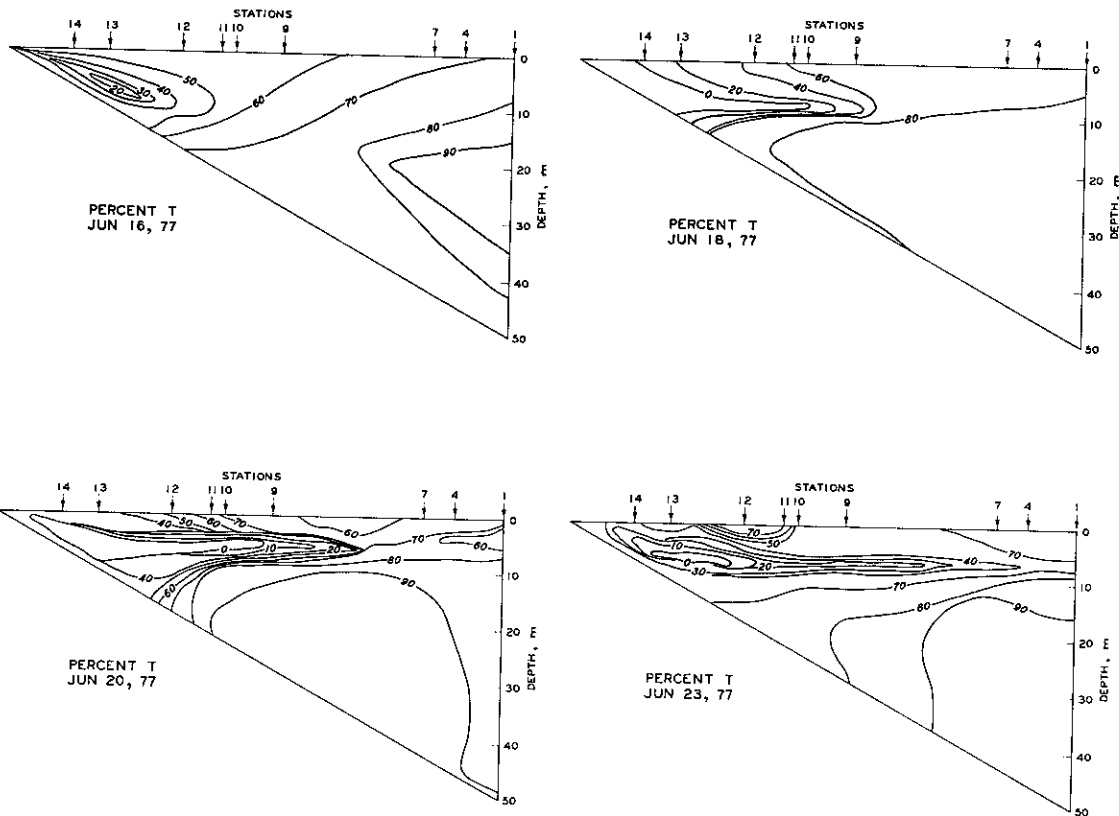
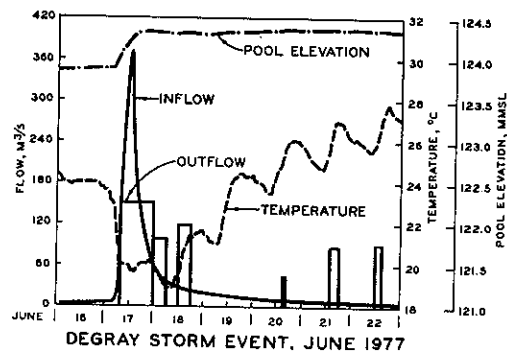


Figure B2. June 1977 storm event, DeGray Lake, Arkansas (Percent T is percent transmittance).

$$\epsilon_i = \frac{\Delta \rho_i}{\rho_a} = \frac{996.288 - 995.733}{995.733} = 5.6 \times 10^{-4}$$

3. The plunge point depth is computed from Equation (18) (Savage and Brimberg 1975):

$$h_p = \left(\frac{q^2}{g \epsilon_i F_p^2} \right)^{1/3}$$

where

$$F_p = \frac{2.05}{(1+\alpha)} \left(\frac{S}{f_b} \right)^{0.478} = \frac{2.05}{(1+0.2)} \left(\frac{0.0012}{0.02} \right)^{0.478} = 0.45$$

Therefore,

$$h_p = \left(\frac{(4.6/70)^2}{9.8 * 5.6 \times 10^{-4} * (0.45)^2} \right)^{1/3} = 1.6 \text{ m}$$

The width of the zone of conveyance was 70 m, which was the bank-full width of the old river channel (Figure 6). The observed hydraulic plunge point depth was 1.8 m.

4. The initial mixing coefficient is computed from Equation (32) and the downstream densimetric Froude number from Equation (44)

$$\left(R_n = 1/F_n^2 \right)$$

$$F_n^2 = \frac{2S_2S}{\frac{1}{2}S_1\beta + f_t + \left[\left(\frac{1}{2}S_1\beta + f_t \right)^2 + 4\beta S_2S \right]^{1/2}}$$

where $S_1 = 0.25$, $S_2 = 0.75$, and $\beta = 0.0015$ are site-independent coefficients. Therefore, for any specific reservoir the mixing coefficient and downstream densimetric Froude number are constant such that

$$F_n^2 = \frac{2(0.75)(1.2 \times 10^{-3})}{\frac{1}{2}(0.25)(0.0015) + 0.024 + 0.024}$$

where

$$\left[\left(\frac{1}{2}(0.25)(0.0015) + 0.024 \right)^2 + 4(0.0015)(0.75)(1.2 \times 10^{-3}) \right]^{\frac{1}{2}} = 0.024$$

and

$$F_n = 0.19$$

From Equation (32), the mixing coefficient is

$$\gamma = 1.2F_n - 0.2 = 1.2(0.19) - 0.2 = 0.03$$

which is low compared to the measured value of 0.10. The revised flow rate and inflow temperature after mixing are:

$$Q_{bo} = (1 + \gamma)Q_i = (1.03)(4.6) = 4.7 \text{ m}^3/\text{sec}$$

$$T_{bo} = \frac{\gamma T_a + T_i}{1 + \gamma} = \frac{(0.03)(29.8) + 27.9}{1.03} = 28.0^\circ\text{C}$$

5. The centerline depth of the interflow is determined by comparing the inflow temperature (density) with a measured temperature (density) profile in the lake (Figure B3). The centerline depths for $\gamma = 0$, $\gamma = 0.03$, and $\gamma = 0.10$ are 5.9, 5.7, and 5.5 m, respectively. The observed centerline depth was approximately 5.5 m. It should be noted, however, that the inflow temperature varied from 27.4° to 28.4°C during the period of dye injection. This range corresponds to the depth range 5.0 to 6.1 m which falls within the inflow zone (Figure B3).

6. Using a centerline depth of 5.5 m ($\gamma = 0.10$), the upper and lower limits of the inflow are determined from Equation (54) assuming

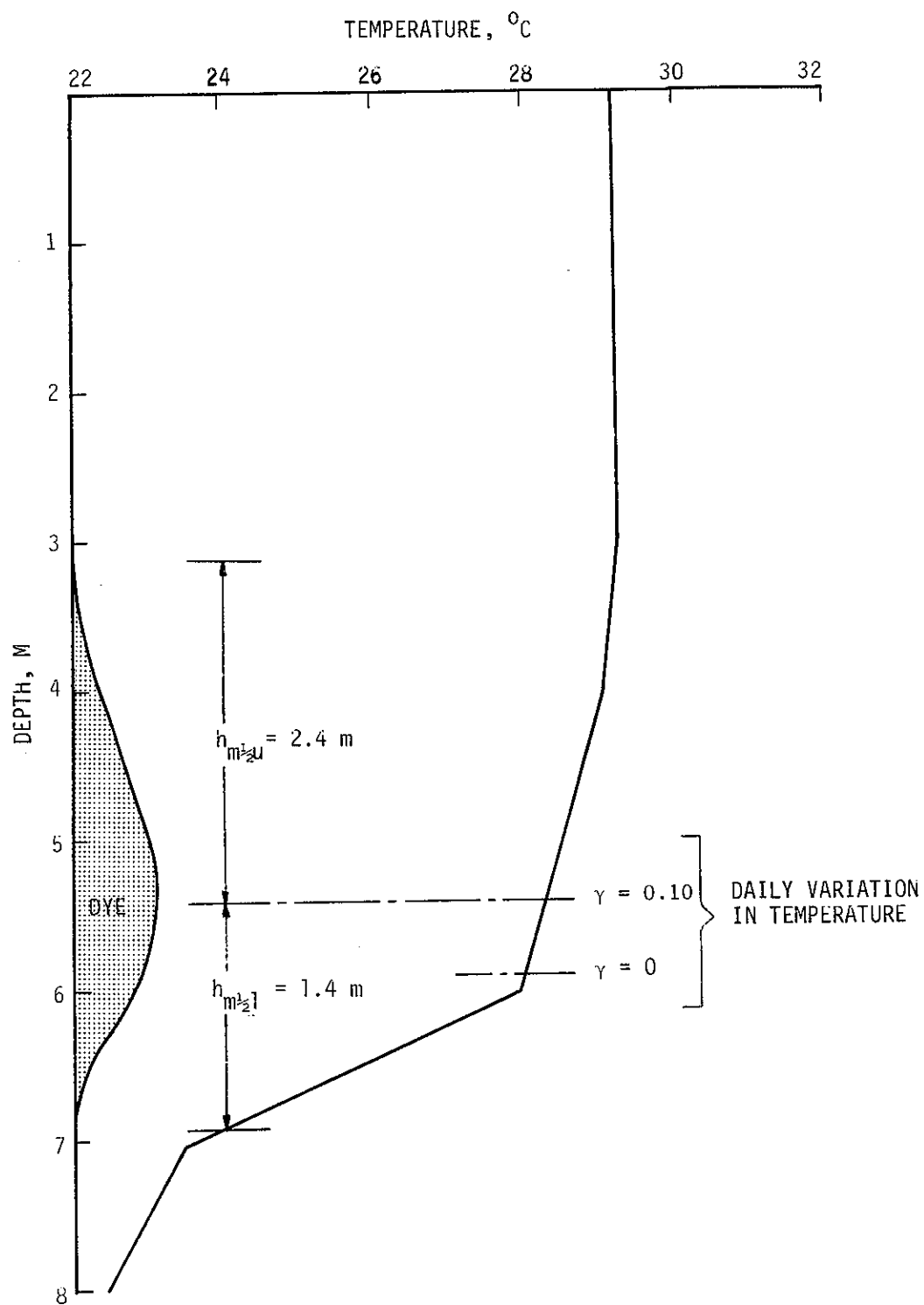


Figure B3. Comparison of predicted and observed interflow placement and thickness, July 1979 dye study, DeGray Lake, Arkansas.

one-half of the flow is distributed above the centerline and one-half below the centerline depth. Therefore,

$$h_{m/2u} = 2.99 \left(\frac{(Q_{bo}/(2W))^2}{\frac{g \Delta \rho_u}{\rho}} \right)^{1/3}$$

where $Q_{bo} = 5.06 \text{ m}^3/\text{sec}$ and $W = 70 \text{ m}$ (i.e., the width of the zone of conveyance). Since $\Delta \rho_u$ is dependent on $h_{m/2u}$, this equation is solved by first selecting an $h_{m/2u}$, then determining $\Delta \rho_u$ from Figure B3 and solving for $h_{m/2u}$. This procedure is continued until the calculated $h_{m/2u}$ converges on the initial $h_{m/2u}$. For example, initially select $h_{m/2u} = 2.1 \text{ m}$. The temperature at $z = 5.5 - h_{m/2u} = 3.4 \text{ m}$ is 29.1°C , and $\rho(29.1^\circ) = 995.941 \text{ kg/m}^3$. Therefore, $\Delta \rho_u/\rho = (996.202 - 995.941)/996.202 = 2.62 \times 10^{-4}$ and $h_{m/2u} = 2.4 \text{ m}$. Since 2.4 m is not similar to 2.1 m , the computation is repeated using $h_{m/2u} = 2.3 \text{ m}$. The temperature and density at the upper limit are now 29.2°C and 995.912 , respectively. Therefore $\Delta \rho_u/\rho = 2.91 \times 10^{-4}$ and $h_{m/2u} = 2.3 \text{ m}$. The lower limit is similarly computed. First, select $h_{m/2l} = 0.9 \text{ m}$, which corresponds to a temperature of 26.2°C and density of 996.756 kg/m^3 . Since the computed $h_{m/2l}$ is 1.9 m and not similar to the initial $h_{m/2l}$ of 0.9 m , the procedure is repeated with $h_{m/2l} = 1.4 \text{ m}$. This half-thickness corresponds to a temperature of 24.0°C and density of 997.323 kg/m^3 . Solving for $h_{m/2l}$ results in 1.5 m , which is similar to the 1.4 m initially selected. The total thickness of the interflow is $1.4 \text{ m} + 2.4 \text{ m} = 3.8 \text{ m}$, which agrees with the vertical dye distribution (Figure B3).

7. The speed at which the interflow propagates into the reservoir is given by Equation (53):

$$u_m = 0.194 \sqrt{\frac{\Delta \rho}{\rho} g h_m}$$

where $\Delta\rho$ and h_m are over the total thickness of the interflow. Therefore, $\Delta\rho = 1.41 \text{ kg/m}^3$, $\rho_m = 996.202 \text{ kg/m}^3$, $h_m = 3.8 \text{ m}$ and $u_m = 0.045 \text{ m/s} = 4.5 \text{ cm/s}$. The leading edge of the dye plume was observed to advance at 3.3 cm/s .

June 1977 Storm Event

8. All of the predictive equations reviewed in this report assumed steady state. In this example, they are applied to an unsteady storm event (Figure B2) to determine their accuracy. The required data are:

Flow rate $Q_i = 370 \text{ m}^3/\text{s}$

Inflow temperature $T_i = 19.9^\circ\text{C}$

Inflow density $\rho_i(19.9^\circ) = 998.251 \text{ kg/m}^3$

Ambient lake temperature $T_a = 28.2^\circ\text{C}$

Ambient lake density $\rho_a(28.2) = 996.202 \text{ kg/m}^3$

Other coefficients and parameters which are site-specific and/or invariant include:

Total friction coefficient $f_t = 0.024$

Bottom slope $S = 1.2 \times 10^{-3}$

Conveyance width $W_c = 440 \text{ m}$

Profile constant $S_1 = 0.25$

Profile constant $S_2 = 0.75$

Entrainment coefficient $\beta = 0.0015$

9. In this example, the plunge depth is computed using the equations of Savage and Brimberg (1975) (Equation 18) and Hebbert et al. (1979) (Equation 20). Since the densimetric Froude number F_p used in the Savage and Brimberg equation is invariant for a specific reservoir, $F_p = 0.45$ from paragraph 3. Therefore, the Savage and Brimberg plunge depth is

$$h_p = \left(\frac{q^2}{g \epsilon_i F_p^2} \right)^{1/3} = \left(\frac{(370/440)^2}{(9.8 * 0.002 * 0.45^2)} \right)^{1/3} = 5.5 \text{ m}$$

where

$$\epsilon_i = \frac{\Delta \rho_i}{\rho_a} = \frac{998.251 - 996.202}{996.202} = 0.002$$

The Hebbert et al. formulation assumes a triangular cross section and the site-specific densimetric Froude number is given by Equation (19):

$$F_n^2 = \frac{\sin S \tan \phi}{C_D} (1 - 0.85 C_D^{1/2} \sin S)$$

where

C_D = total drag coefficient.

Substituting the site-specific characteristics for DeGray Lake yields

$$F_n = \left[\frac{\sin(0.0012) \tan(85^\circ)}{0.055} (1 - 0.85(0.055)^{1/2} \sin(0.0012)) \right]^{1/2} = 0.5$$

and the equation for the plunge depth (Equation 20) becomes

$$h_p = 0.57 \left(\frac{Q_i^2}{g \epsilon_i} \right)^{1/5}$$

Substituting $\epsilon_i = 0.002$ and $Q_i = 370 \text{ m}^3/\text{sec}$ yields 13.3 m, which must be divided by 2 to obtain the hydraulic depth for a triangular cross section. Therefore, $h_p = 13.3/2 = 6.7 \text{ m}$, which is comparable to the 5.5 m computed from Savage and Brimberg and the observed hydraulic depth of 5.4 m. These two computations indicate the differences in magnitude that can be obtained from the different formulations for the plunge depth. It is also worth noting that the densimetric Froude number required for both formulations differ slightly (i.e., 0.45 versus 0.50).

10. Since the downstream densimetric Froude number computed from Equation (44) is site specific and not directly a function of flow, the computed initial mixing coefficient for this example will be the same as the previous example (i.e., $\gamma = 0.03$). This value compares with a measured mixing coefficient of 0.07.

11. Assuming no initial mixing and an inflow temperature of 19.9°C , the centerline of the intrusion would be at an elevation of 116.7 m (Figure B4). With an initial mixing coefficient of 0.07 and a surface temperature of 29°C , the revised inflow temperature would be 20.5°C and the centerline of the intrusion would be at 117.0 m. As shown in Figure B2, the inflow temperatures varied from approximately 19°C to 24°C during the period of elevated flow and, assuming no mixing, would have entered the reservoir as separate intrusions between the elevations of 116.3 and 119.1 m. This zone closely approximates the intrusion thickness (Figure B4). For the intrusion computations, a centerline at 117.0 m will be assumed.

12. The flow rate required for the intrusion thickness computation (i.e., Equation 54) must be averaged over the time scale given by Equation (53):

$$t_s = \frac{L}{0.194 \left(\frac{\Delta\rho_m}{\rho} g h_m \right)^{1/2}}$$

where

L = reservoir length

$\Delta\rho_m$ = density change across metalimnion

h_m = average thickness of metalimnion

For DeGray Lake, under average summer stratification conditions, $L = 32,000$ m, $h_m = 8$ m, $\Delta\rho_m = \rho(25^{\circ}\text{C}) \approx 3 \text{ kg/m}^3$, and

$$t_s = \frac{32,000}{0.194 \left(\frac{3}{1000} * 9.8 * 8 \right)^{1/2}} = 3.4 \times 10^5 \text{ sec} = 3.9 \text{ days}$$

The resultant average flow rate for period 16-19 June was $63 \text{ m}^3/\text{sec}$.

13. The upper and lower half-thicknesses are determined from Equation (54), using a centerline elevation of 117 m and an average flow rate of $63 \text{ m}^3/\text{sec}$. For the upper half-thicknesses $h_{m/2u}$ first

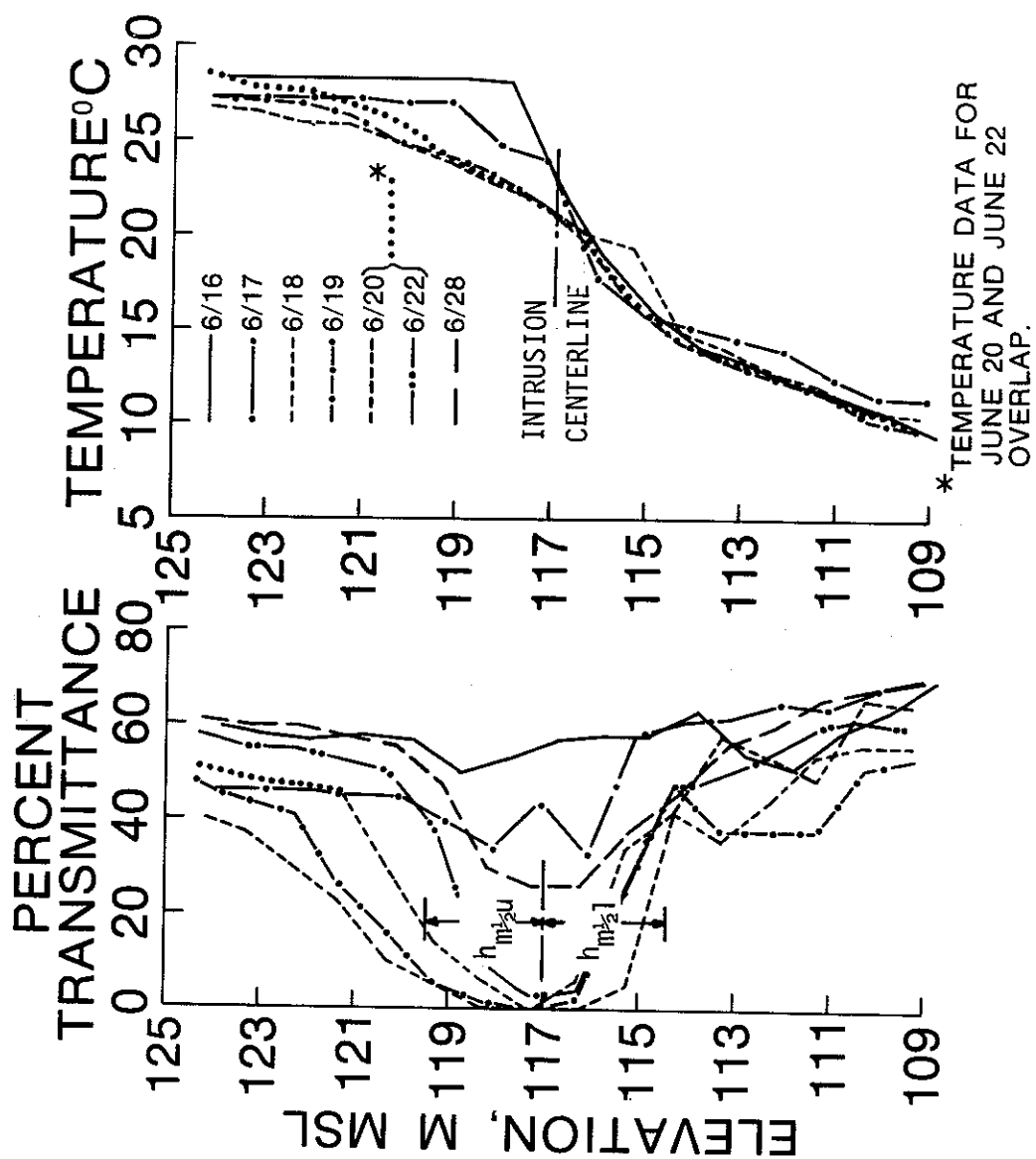


Figure B4. Comparison of predicted and observed interflow placement and thickness, June 1977 storm event, DeGray Lake, Arkansas.

assume $h_{m/2u} = 3$ m. From the temperature profile on 19 June (Figure B4), $\Delta\rho_m/\rho = (\rho(20.5^\circ) - \rho(26.2^\circ))/\rho(20.5^\circ) = (998.126 - 996.756)/998.126 = 1.37 \times 10^{-3}$. Therefore,

$$h_{m/2u} = 3.0 \left(\frac{(63/440/2)^2}{9.8 \times 0.00137} \right)^{1/3} = 2.2 \text{ m}$$

Since $2.2 < 3.0$ m, try $h_{m/2u} = 2.6$ m, which intersects the temperature profile at 25.3°C . Therefore, $\Delta\rho_m/\rho = (\rho(20.5^\circ) - \rho(25.3^\circ))/\rho(20.5^\circ) = 1.14 \times 10^{-3}$, and $h_{m/2u} = 2.3$ m. Since the predicted $h_{m/2u}$ is still less than the assumed $h_{m/2u}$, (i.e., $2.3 < 2.6$ m), try $h_{m/2u} = 2.4$ m. In this case, $\Delta\rho_m/\rho = (\rho(20.5^\circ) - \rho(24.7^\circ))/\rho(20.5^\circ) = 9 \times 10^{-4}$, and $h_{m/2u}$ converges to 2.5 m. For the lower half-thicknesses, first assume $h_{m/2l} = 2.5$ m. Then, from Figure B4, $\Delta\rho_m/\rho = (\rho(14.6^\circ) - \rho(20.5^\circ))/\rho(20.5^\circ) = 1.06 \times 10^{-3}$, and $h_{m/2l} = 2.4$ m, which is similar to the assumed $h_{m/2l}$ of 2.5 m. The computed intrusion zone is shown in Figure B4.

14. The intrusion speed is computed from Equation (53)

$$u_m = 0.194 \sqrt{\frac{\Delta\rho_m}{\rho} g h_m}$$

using $h_m = h_{m/2u} + h_{m/2l}$ and $\Delta\rho_m$ across h_m . Substituting $h_m = 4.9$ m and $\Delta\rho_m/\rho = 1.96 \times 10^{-3}$ yields $u_m = 0.06$ m/sec, which is the same as the observed speed of 0.06 m/sec.

Discussion

15. The numbers used in the two preceding examples differ slightly from those used in the main text of this report because different in-lake conditions were selected. Figure B4 clearly illustrates the variations that can be expected in temperature and intrusion characteristics. It is therefore important to use in the calculations inflow and in-lake characteristics that were collected at the same time and location.

Because of the dynamic nature of these characteristics, differences in predictions can be expected.

APPENDIX C: COMPUTER ALGORITHM

1. This appendix outlines a mathematical inflow algorithm to be used in a one-dimensional water quality model such as CE-QUAL-R1 (Environmental Laboratory 1982) to predict inflow placement, plunge point depth, initial mixing, underflow entrainment, and intrusion thickness. The algorithm is based on the formulations recommended in the main text of this report and considers a reservoir to be composed of n horizontal layers of variable thickness $\Delta z(k)$ and variable density $\rho(k)$ where $k = 1, n$. The layers are numbered from the bottom ($k = 1$) to the water surface ($k = n$). The algorithm requires the following information for each tributary:

- a. Inflow rate Q_i , m^3/sec .
- b. Inflow density ρ_i , kg/m^3 . (This should be a function of temperature, TDS, and SS. See Appendix A.)
- c. Conveyance width $W(k)$ for each horizontal layer k , m (should be representative of main body of reservoir).
- d. Bottom slope S , m/m (computed from reservoir depth Z_m , and length L along the old thalweg: $S = Z_m/L$).
- e. Half angle ϕ representative of the upper end of the reservoir (see Figure 21).
- f. Total friction coefficient for underflow f_t ($f_t = f_b + f_i$).
- g. Upper mixed layer depth Z_{mix} , m (composed of layers, $k = m, n$).

2. For each tributary, the following computational steps are required:

- a. Compute the plunge point depth h_p using the formulation of Hebbert et al. (1979), (Equation 20):

$$h_n = \left(\frac{2Q_i}{F_p^2 g \epsilon_i \tan^2 \phi} \right)^{1/5} \quad (C1)$$

where

$$F_p^2 = \frac{\sin S \tan \phi}{C_D} (1 - 0.85 C_D^{1/2} \sin S) \quad (C2)$$

and $\epsilon_i = \text{ABS}[(\rho_s - \rho_i)/\rho_s]$

ρ_s = reservoir water surface density, kg/m^3

$C_D = f_t/4$

Determine the layers in the plunge zone (i.e., $k = p, n$ where p is the layer at depth h_p).

- b. Compute the initial mixing coefficient, γ , using the formulation of Jirka and Watanabe (1980) (Equation 32) and the densimetric Froude number computed from Equation (C2):

$$\gamma = 1.2 F_p - 0.2 \quad (C3)$$

- c. Compute the revised rate Q_{bo} and density ρ_{bo} after initial mixing:

$$Q_{bo} = Q_i (1 + \gamma) \quad (C4)$$

and

$$\rho_{bo} = \frac{\gamma \rho_s + \rho_i}{(1 + \gamma)} \quad (C5)$$

- d. If $\rho_{bo} < \rho_s$, a density overflow occurs.
- (1) If $h_p > Z_{mix}$ (i.e., $p < m$), distribute the inflow Q_i throughout the depth Z_{mix} ($k = m, n$), assuming a maximum velocity at the water surface and a lower inflow zone limit m . No initial mixing occurs since it is assumed F_p is small (< 1) and the density gradient at the bottom of the mixed layer is sufficiently strong to inhibit mixing and force the inflow into the mixed layer only.

- (2) If $h_p < z_{mix}$ (i.e. $p > m$), distribute the inflow rate after initial mixing Q_{bo} throughout the depth h_p ($k = p, n$), assuming a maximum velocity at the water surface and a lower inflow zone limit p (Figure C1).

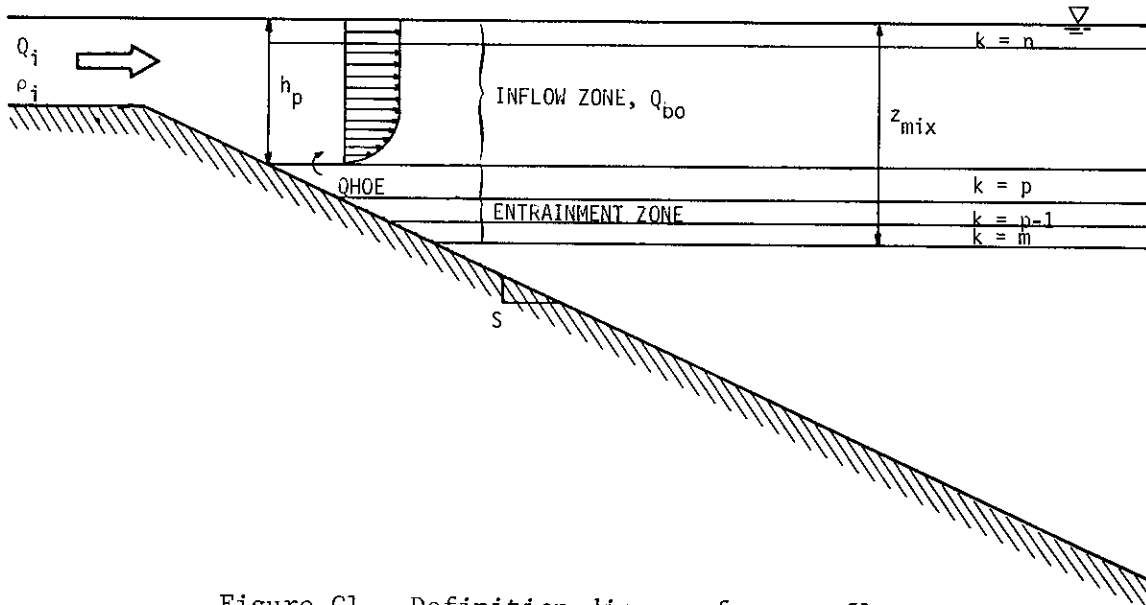


Figure C1. Definition diagram for overflow.

In this case, the entrained inflow ($Q_{bo} - Q_i$) and associated constituents are entrained from layers m through $p - 1$, in proportion to their thickness:

$$QHOE(k) = (Q_{bo} - Q_i) \frac{\Delta z(k)}{(z_{mix} - h_p)} \quad (C6)$$

where

$QHOE(k)$ = entrained inflow from layer k , m^3/sec .

$\Delta z(k)$ = thickness of layer k , m

In this algorithm, it is assumed $F_n < 1$ and ϵ_i for an overflow is small. Thermal discharges are not considered.

e. If $\rho_{bo} > \rho_s$, a density underflow occurs

- (1) Compute the densimetric Froude number F_n and the normal depth of flow for the underflow from Equation (44)

$$F_n^2 = \frac{2S_2S}{\frac{1}{2}S_1\beta + f_t + ((\frac{1}{2}S_1\beta + f_t)^2 + 4\beta S_2S)^{1/2}} \quad (C7)$$

where

$$S_2 = 0.75 \text{ (from Ellison and Turner 1959)}$$

$$S_1 = 0.25 \text{ (from Ellison and Turner 1959)}$$

$$\beta = 0.0015 \text{ (from Ashida and Egashira 1977)}$$

Since F_n is a constant, the normal depth of flow for a rectangular channel of width W_r immediately below the plunge zone is estimated by (Equation 29):

$$h_b = \frac{1}{F_n^2} \left(\frac{(Q_{bo}/W)^2}{\frac{\Delta\rho_b}{\rho_{bo}} g} \right)^{1/3} \quad (C8)$$

where

$$W_r = \text{bank-full width of old river channel, m}$$

$$\Delta\rho_b = \rho_{bo} - \rho_e, \text{ kg/m}^3$$

$$\rho_e = \left[\sum_{k=j}^n \rho(k)\Delta z(k) \right] / \gamma h_p = \text{entrained density, kg/m}^3.$$

and ρ_{bo} is given by Equation (C5).

The entrainment zone is estimated to be γh_p , which is composed of layers $k = j, n$ (Figure C2). If $\gamma h_p < \Delta z(n)$, then $\gamma h_p = \Delta z(n)$.

- (2) For each layer below j the entrainment and increase in underflow thickness h_b is computed until the

$$Q_e(k) = Q_b(k) - Q_{bo}(k) \quad (C12)$$

Equations (C9), (C10), (C11), and (C12) are recomputed for each layer until $\rho_b(k) < \rho(k)$, then an intrusion occurs with layer k as the layer of neutral buoyancy.

- f. The thickness of intrusion is determined from Equation (54). Since the vertical density gradient in the vicinity of an intrusion is usually nonlinear (Figure C3), the intrusion

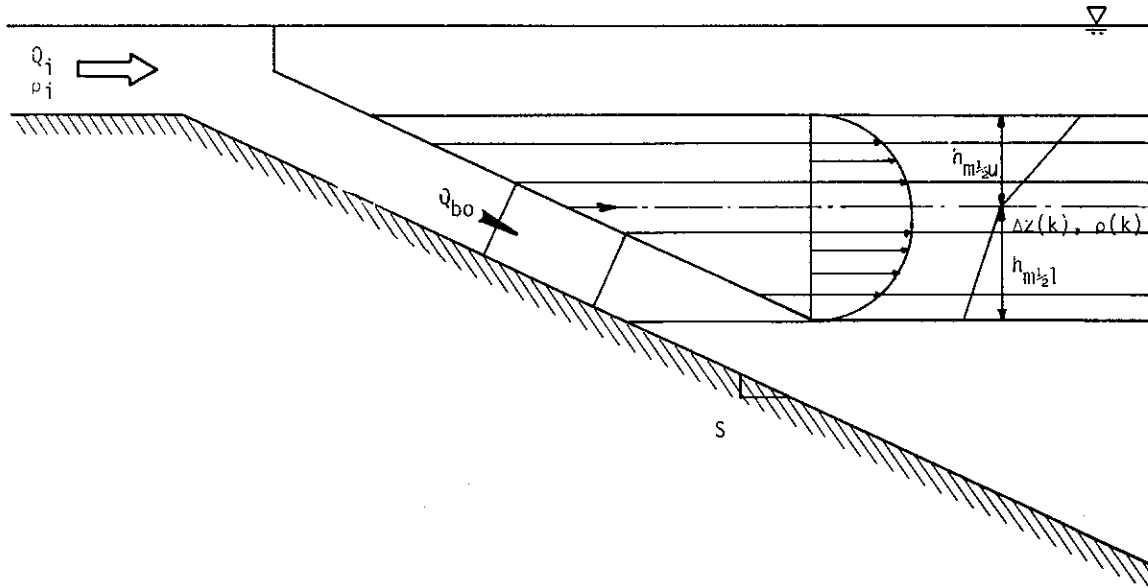


Figure C3. Definition diagram for an interflow.

thickness computation is separated for the upper and lower limits. The upper half-thickness is therefore:

$$h_{m2u} = 3.0 \left(\frac{(Q_{bo}(k)/(2W(k)))^2}{\frac{g\Delta\rho_u}{\rho(k)}} \right)^{1/3} \quad (C13)$$

where

- k = number of layer that intrusion enters
 $Q_{bo}(k)$ = total inflow rate with all entrainment, but averaged over the appropriate time scale, m^3/sec
 $W(k)$ = width of layer k , m
 $\Delta\rho_u$ = density difference over the half-thickness $h_{m/2u}$, kg/m^3

$Q_{bo}(k)$ must be divided by 2 in Equation (C13) since it is assumed that half the flow is above the level of neutral buoyancy and half below. $Q_{bo}(k)$ must also be averaged over the time scale

$$t_s = \frac{Z_m}{0.194 \left(\frac{\Delta\rho_m}{\rho} g h_m \right)^{1/2}}$$

where $\Delta\rho_m$ is the change in density across a metalimnion of thickness h_m . Equation (C13) is solved with

$$\Delta\rho_u = \rho(k+i) - \rho(k)$$

$$h_{m/2u} = \sum_{i=1}^m (\Delta z(k-l+i) + \Delta z(k+i))/2$$

adding one layer at a time until

$$ABS \left[h_{m/2u} - 3.0 \left(\frac{(Q_{bo}(k)/(2W(k)))^2}{\frac{g\Delta\rho_u}{\rho(k)}} \right)^{1/3} \right] \leq \frac{\Delta z}{2}$$

where $\overline{\Delta z}$ = average layer thickness, m

The lower limit is determined in a similar manner.

- g. The interflows and overflows are distributed between upper and lower limits according to parabolic velocity profiles used in selective withdrawal.

APPENDIX D: NOTATION

- A = cross-sectional area, m^2
 B = top width of the underflow, m^2
 C_b = bottom drag coefficient
 C_D = total drag coefficient
 C_P = coefficient to account for nonhydrostatic pressure distribution
 C_{SS} = SS concentration, g/m^3
 C_{TDS} = TDS concentration, g/m^3
 E = entrainment coefficient
 F_b = underflow densimetric Froude number = $\frac{u_b}{(\epsilon_b g h_b)^{1/2}}$
 F_i = inflow densimetric Froude number = $\frac{u_i}{(\epsilon_i g h_i)^{1/2}}$
 F_m = internal densimetric Froude number = $q_m / N_m L_m^2$
 F_n = normal depth densimetric Froude number
 F_p = densimetric Froude number at plunge point
 f_b = bed friction coefficient
 f_i = interfacial friction coefficient
 f_t = total friction factor = $f_b + f_i$
 Gr = Grashof number = $N_m^2 L_m^4 / \kappa_v^2$
 g = gravitational acceleration, m^2/sec
 g' = relative acceleration of gravity = $\frac{\rho_b - \rho_a}{\rho_a} g$, m^2/sec
 h_1 = observed plunge depth, m
 h_2 = observed depth of underflow, m
 h_b = depth (thickness) of underflow, m
 h_{bo} = initial depth of underflow, m
 h_c = critical depth = $\left(\frac{q_i^2}{g \epsilon_i} \right)^{1/3}$, m

h_i	= inflow depth, m
h_m	= intrusion thickness, m
h_{m2l}	= lower intrusion thickness, m
h_{m2u}	= upper intrusion thickness, m
h_n	= downstream normal depth, m
h_p	= plunge point (separation) depth, m
h_s	= thickness of the underflowing/overflowing current, m
K	= constant = f_t/S_2
L	= length of reservoir, m
L_m	= intrusion length, m
L_s	= overflow length, m
m	= lower uptake zone limit
N_p	= dimensionless ratio = h_p/h_n
N_c	= dimensionless ratio = h_c/h_n
N_m^2	= buoyancy frequency averaged over intrusion thickness h_m , sec^{-2}
p	= pressure, bars (1 bar \approx 10.2 m of water)
Pr	= Prandtl number = κ_v/κ_T
Q	= discharge, m^3/sec
Q_b	= underflow discharge, m^3/sec
Q_{bo}	= revised flow rate including entrainment, downstream of the plunge point, m^3/sec
Q_e	= rate of entrainment flow, m^3/sec
Q_i	= original inflow rate, m^3/sec
$Q_{HOE}(k)$	= entrained inflow from layer k , m^3/sec
q_i	= unit width discharge, $\text{m}^3/\text{m}/\text{sec}$
q_m	= inflow per unit width at takeoff point after entrainment, $\text{m}^3/\text{m}/\text{sec}$
R	= dimensionless parameter = $F_m Gr^{1/3}$
R_n	= normal depth Richardson number

Ri = Richardson number = $\frac{g'h_b}{u_b^2}$
 r = entrance mixing ratio
 S = bottom slope
 SG = specific gravity of the suspended solids
 S_1, S_2 = profile constants
 T = water temperature, °C
 T_a = lake surface temperature, °C
 T_i = inflow temperature, °C
 T_{bo} = inflow temperature after mixing, °C
 t = time, sec
 u_b = underflow velocity, m/sec
 u_{bo} = initial underflow velocity, m/sec
 u_i = inflow velocity = q_i/h_i , m/sec
 u_m = intrusion speed = L_m/t , m/sec
 u_p = velocity at the plunge point, m/sec
 u_s = propagation speed of the overflow front, m/sec
 W = width, m
 W_c = width of zone of conveyance, m
 W_o = initial width, m
 W_r = bank-full width of old river channel, m
 W_x = width at distance x , m
 x = distance from source, m
 x_o = reference point for beginning of underflow, m
 z = reservoir depth, m
 Z_m = maximum reservoir depth, m
 Z_{mix} = depth of upper mixed layer, m
 α = ratio of interfacial to bed friction = f_i/f_o
 β = coefficient in entrainment equation
 γ = initial mixing coefficient
 $\overline{\Delta z}$ = average layer thickness, m
 $\Delta z(k)$ = thickness of layer k , m

$\Delta\rho_b$	= density difference of ambient and underflow, kg/m^3
$\Delta\rho_i$	= density difference between receiving water and inflow = $(\rho_a - \rho_i)$, kg/m^3
$\Delta\rho_m$	= change in density over h_m , kg/m^3
$\Delta\rho_{SS}$	= density increment due to suspended solids, kg/m^3
$\Delta\rho_{TDS}$	= density increment due to total dissolved solids, kg/m^3
ϵ_b	= relative density difference = $\Delta\rho_b/\rho_a$
ϵ_i	= relative density difference = $\Delta\rho_i/\rho_a$
κ_T	= average vertical diffusivity of heat, m^2/sec
κ_v	= average vertical eddy viscosity, m^2/sec
ζ	= ratio of normal depth to plunge point depth = h_n/h_p
$\eta^3 C_\kappa$	= mixing efficiency
θ	= bed angle
λ	= $\alpha/(1 + \alpha)$
$\rho(k)$	= density of layer k, kg/m^3
$\rho(z)$	= density variation with depth, kg/m^3
ρ_a	= ambient density of the reservoir surface waters, kg/m^3
ρ_b	= density of the underflow, kg/m^3
ρ_{bo}	= revised inflow density after entrainment at the plunge point, kg/m^3
ρ_e	= entrainment density, kg/m^3
ρ_i	= density of inflowing water, kg/m^3
ρ_m	= density of intrusion, kg/m^3
ρ_s	= density of reservoir surface waters, kg/m^3
ρ_T	= water density resulting from temperature variations, kg/m^3
ρ_{TDS}	= density conversion factor, $\text{kg/m}^3/\text{g/m}^3$
ρ_w	= water density, kg/m^3
ϕ	= half-angle of the triangular cross section